Lawrence Berkeley National Laboratory

Title
THE TWO-DIMENSIONAL TRIANGULAR LATTICE AND ITS APPLICATION TO LITHIUM-INTERCALATED LAYERED COMPOUNDS

Permalink
https://escholarship.org/uc/item/3xh3c8w1

Author
Cerqueira, R. Osorio de

Publication Date
1982-08-01

Lawrence Berkeley Laboratory
UNIVERSITY OF CALIFORNIA

Materials & Molecular Research Division

THE TWO-DIMENSIONAL TRIANGULAR LATTICE AND ITS
APPLICATION TO LITHIUM-INTERCALATED LAYERED
COMPOUNDS

Roberto Osório de Cerqueira
(Ph.D. thesis)

August 1982

THE TWO-DIMENSIONAL TRIANGULAR LATTICE AND ITS APPLICATION TO LITHIUM-INTERCALATED LAYERED COMPOUNDS

Roberto Osório de Cerqueira

Ph.D. Thesis

August 1982

Materials and Molecular Research Division
Lawrence Berkeley Laboratory
University of California
Berkeley, CA 94720

ABSTRACT

THE TWO-DIMENSIONAL TRIANGULAR LATTICE AND ITS APPLICATION

TO LITHIUM-INTERCALATED LAYERED COMPOUNDS

by Roberto Osório de Cerqueira

The triangular lattice gas is examined as a model for lithium intercalation in transition-metal dichalcogenides. Order-disorder phase diagrams for the lithium atoms and thermodynamic functions are computed by means of the cluster-variation method in its single-site (mean-field) and triangle approximations.

The single-site three-sublattice approximation with nearest-neighbor interactions is examined first. It gives the correct physical picture for features of the incremental capacity versus concentration curves of systems like Li_xTiS_2. It is found that minima are associated with ordered structures and sharp maxima (divergences) are caused by the coexistence of ordered and disordered phases over small concentration intervals.

The triangle approximation, with two-particle repulsions and three-particle attractions, is discussed. It accounts for values of x where peaks in the incremental capacity of Li_xTiS_2 are observed.

Finally a single-site approximation is applied to a model with different site energies randomly distributed over the lattice. It is intended to represent intercalated Li in $Li_xTa_yTi_{1-y}S_2$. Ground-state diagrams--in the space of x

and a site energy parameter--show different sequences of ordered phases. Finite-temperature results show additional minima in the incremental capacity curves due to nearly complete filling of chemical types of sites. The model is good for values of $\underline{y}$ where the experimental results suggest a disordered distribution of Li atoms.

Para Esther
e Felipe

ACKNOWLEDGEMENTS

CONTENTS

I. THE MATERIALS AND THE MODEL

A. INTRODUCTION

Good rechargeable batteries are being searched for use
in electric vehicles and in energy storage during off-peak
consumption periods and from solar sources.[1,2] These
batteries should be able to undergo at least about 10^3
recharge cycles, should have an energy density[3] greater
than 10^2 watts-hour/kg and, of course, should be economic-
ally viable.

The interest in lithium intercalation compounds has
been recently enhanced by the search for such batteries. The
choice of lithium as the intercalated species is a natural one,
due to its lowest mass among the metals and high reactivity.[4]

Among the layered intercalation materials, the most
extensively studied in the past have been the graphite[2,5]
compounds. The free energy of formation of lithium-graphite
compounds, however, is too small to provide a sufficient
voltage for a practical battery.

On the other hand, the process of intercalation of
lithium in several transition-metal dichalcogenides can
provide an emf of several volts. The progress achieved
in the last decade[4,6] in the investigation of these inter-
-calates has been facilitated by the availability of the
dichalcogenides as single crystals and by their chemical
stability.

The following sections of this chapter will focus on

the transition-metal dichalcogenides and their Li inter-
calates, with emphasis on the $Li_xTa_yTi_{1-y}S_2$ series. The
interactions between the Li atoms and the applicability of
a lattice gas model to the problem of ordering of these
atoms will be discussed next.

Chapter II presents a formulation of the cluster-variation
approximation to the lattice gas problem. The single-site
and the nearest-neighbor triangle basic clusters are con-
sidered in Chapters III and IV respectively, as models for
Li_xTiS_2. Finally, in Chapter V, a theory is presented for
the effects of a random distribution of different species
of host atoms, as in $Ta_yTi_{1-y}S_2$.

B. LAYERED TRANSITION METAL DICHALCOGENIDES AND
    THEIR INTERCALATES

Layered transition-metal dichalcogenides are compounds
represented by MX_2, where M is a transition metal of groups
IVB (Ti, Zr, Hf), VB (V, Nb, Ta) or VIB (Cr, Mo, W) and X
is a chalcogen of group VIIA (S, Se, Te). In both the
intercalated and non-intercalated forms, the MX_2 compounds
have interesting physical properties[7] that are dominated by
their essentially two-dimensional crystal structure. For
instance, they frequently grow in the form of thin platelets
that can be cleaved into samples with a thickness of only
a few angstroms; their electric and thermal conductivities
are much larger within the basal plane then along the per-
pendicular direction; the formation of charge density waves[8,9]

is favored by essentially cylindrical Fermi surfaces typical
of two-dimensional systems.

The structure of the MX_2 compounds[6,9-11] consists of
strongly bound X-M-X sandwiches that are stacked one on
another and separated by considerably weaker van der Waals
gaps. In each M or X layer the atoms are distributed in
a two-dimensional triangular lattice. The different crystal
structures of the MX_2 compounds can then be described by
means of the ABC stacking notation (where the fcc lattice
is described by the ABC unit and the hcp lattice by the AB
unit). We denote the positions of the X atoms by capital
letters and the position of the M atoms by lowercase letters.
The most common structures are then the 1T polytype of TiS_2
(with unit sequence AbC) and the 2H polytypes of NbS_2 (AbA CbC)
and of MoS_2 (AbA BaB). In the 1T polytype the metal atoms
have an octahedral coordination of six chalcogens while in
the 2H polytypes they have trigonal prismatic coordination.

Band-structure calculations[7,12] have been performed
for several of the transition-metal dichalcogenides. A
schematic illustration of the density-of-states distribution
for the 1T polytypes of the MX_2 compounds is given in Fig. 1.1.
For metal atoms of the group IVB, a small gap separates
completely filled bands, derived predominantly from the p
orbitals of the X atom, from completely empty d bands. This
leads to a semiconductor behavior, such as the one observed[13]
in TiS_2, where the band gap is of the order of 0.5 eV. On

the other hand, for metal atoms of the group VB the additional electron partially fills the $\underline{d}$ band, which leads to metallic behavior at high temperatures[14] for the 1T form of TaS_2. This compound, however, also becomes a semiconductor below a critical temperature of about 350 K due to additional band gaps caused by charge-density waves.[8]

Several types of monoatomic species and organic and inorganic molecules[15] have been successfully intercalated into the van der Waals gaps of the transition metal dechalcogenides. The sites available for intercalation of atoms, denoted by lowercase letters in parenthesis, are usually the octahedral sites [C(b)A] or the tetrahedral sites [C(a)A or C(c)A]. The octahedral sites form a triangular lattice with nearest-neighbor separation $\underline{a}$ (the lattice constant for the M or X triangular layer) while the projection of the tetrahedral sites (not exactly coplanar) on the basal plane forms a honeycomb hexagonal lattice with nearest-neighbor distance $\underline{a}/\sqrt{3}$.

Among such intercalation materials, Li_xTiS_2 has been the most extensively studied. In this dissertation we will concentrate on the range $0 \leq x \leq 1$, where neutron diffraction experiments[16] indicate that the Li atoms preferentially occupy the octahedral sites. Recent measurements[17] suggest an occupation of the tetrahedral sites at the level of only a few percent for $x > 0.5$, while essentially no tetrahedral sites are occupied for smaller concentrations. Lithium has

also been successfully intercalated[18] for $1 \leq x \leq 3$, with a predominant occupation of the tetrahedral sites.

Intercalation frequently causes dramatic changes in the physical properties of the host lattice. The introduction of alkali metals has been observed[19] to induce metallic behavior in several of the MX_2 compounds. Such metallic behavior in $LiTiS_2$ has been observed by the nuclear magnetic resonance (NMR) experiments of Silbernagel and Whittingham[20] and theoretically confirmed by the band-structure calculation of McCanny,[21] who used a semi-empirical tight-binding method. He interprets the results of intercalation as a predominantly rigid-band, partial filling of the lowest unoccupied states (a Ti $\underline{d}$ band) by a Li electron. The same NMR experiments indicate that the ionization is essentially complete in Li_xTiS_2 for small $\underline{x}$, while 10 to 20% of an electron remains in the neighborhood of a Li atom at $\underline{x}=1$.

Upon intercalation the layers of the host atom move apart and an increase of the interlayer spacing can be observed[22] by X-ray diffraction techniques. An increase of about 10% is observed in the $\underline{c}$ axis from TiS_2 (5.697 Å) to $LiTiS_2$ (6.195 Å), while the $\underline{a}$ axis increases by only 1%. During the intercalation (and removal) process the host matrix retains its structure. This accounts for the very high reversibility of batteries where Li_xTiS_2 is used as a cathode. In the next section we discuss how the electrochemical properties of such batteries can be relevant to

the study of the possibility of ordering of the Li ions for arbitrary values of their concentration $\underline{x}$.

C. THE $Li/Ta_yTi_{1-y}S_2$ BATTERY

The lightest and less expensive of all transition-metal dichalcogenides is TiS_2. It also has the highest Li self-diffusion[23] rate.

The $[Li/TiS_2]$ electrochemical cell consists of a Li anode and a TiS_2 cathode, connected by an external circuit and an electrolyte based on an organic solvent, usually dioxolane-$LiClO_4$. During discharge Li ions travel through the electrolyte and are intercalated in TiS_2, preferentially occupying the interlayer sites of octahedral coordination of six sulfur atoms, while electrons (one per Li ion) travel through the external circuit and are donated to the TiS_2 conduction band. The resulting cell reaction is thus

$$xLi + TiS_2 \rightarrow Li_xTiS_2$$
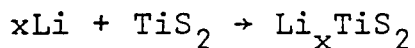
with the following steps[4] taking place:

$$xLi \rightarrow xLi^+ + x\ e^-$$

(on the anode) and

$$xLi^+ + x\ e^- + Ti^{4+}(S^{2-})_2$$

$$\rightarrow Li_x^+\ Ti^{(4-x)+}(S^{2-})_2$$
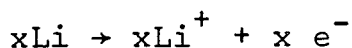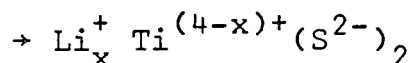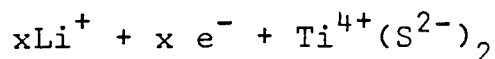
(in the cathode). These cells have a high energy density of 480 watts-hour/kg and are also highly reversible, with essentially no change of structure of the TiS_2 host during discharge and charge.

By means of a new battery cycling technique, which he

calls electrochemical potential spectroscopy,[24] Thompson
has performed accurate measurements[24,25] of the voltage $\underline{V}$
versus concentration $\underline{x}$ relationship in such cells. The
data (Fig. 1.2) show well defined peaks in the incremental
capacity $(-\partial x/\partial V)$ at constant temperature; the main peaks
appear at $x = 1/9$, $1/4$ and $6/7$. Thompson has suggested
that these peaks are associated with the formation of two-
dimensional ordered superlattices of the Li^{+} ions at those
concentrations.

When one electron is transferred from the Li anode to
the $Li_{x}TiS_{2}$ cathode and one Li^{+} ion is simultaneously inter-
calated, the work done on the electron (eV) equals the
change in free energy of the Li^{+} ion between the anode and
the cathode, i.e., the difference between the Li^{+} chemical
potential in the two environments. If the anode is considered
a Li^{+} reservoir, the voltage V is then given by

$$V = \frac{1}{e} (\text{constant} - \mu_1) \quad , \qquad (1.1)$$

where μ_1 is the Li^{+} chemical potential in $Li_{x}TiS_{2}$.

With the use of elementary statistical mechanics,[26]
we can relate the incremental capacity to the mean-square
fluctuation of the Li concentration $\underline{x}$ by

$$- \frac{\partial x}{\partial V} = \frac{Ne}{k_{B}T} <(\Delta x)^{2}> \quad , \qquad (1.2)$$

where $\underline{N}$ is the total number of octahedral sites available for Li occupation in the cathode. Peaks in $(-\partial x/\partial V)$ should therefore be associated with order-disorder phase transitions, where the fluctuations in the composition become appreciable. As we show in the next chapters, these transitions do not usually occur at concentrations where perfectly ordered structures are expected.

Lithium has also been intercalated in the $Ta_yTi_{1-y}S_2$ series[27] ($0 \leq y \leq 1$), of which TiS_2 is a special case. The atoms of Ta and Ti are supposedly randomly distributed in the host compound,[28] which belongs to the 1T polytype. The results for the voltage-composition relations and the incremental capacity curves are plotted in Fig.1.2 for several values of y. The voltage-composition relations show that the voltage is lowered on the Ta-rich end. Smooth incremantal capacity curves suggest absence of Li ordering for $0.1 \leq y \leq 0.5$ while on the Ta-rich end possible divergences indicate formation of two-phase regions.

D. THE LATTICE GAS MODEL AND THE INTERACTIONS BETWEEN INTERCALATE ATOMS

A lattice gas model can be interpreted[29] as a formalism that describes an interstitial solution in a solid as a substitutional solution composed of the interstitial atoms and their vacancies. The lattice is considered rigid, in analogy with the Ising model of magnetism, independently of the concentration of atoms. The Ising model for antiferromag-

netism is mathematically equivalent[30] to the lattice gas
with nearest-neighbor repulsion. Occupied sites are equi-
valent to up spins and vacancies to down spins. The chemical
potential plays the role of the magnetic field and the one-
half-concentration lattice gas can be identified with the
zero-field Ising model. This isomorphism becomes apparent
when we try to relate the grand partition function of the
lattice gas to the partition function of the Ising model.

Several points must be kept in mind in regards to the
applicability of a two-dimensional triangular lattice gas
model to the Li^+ ions intercalated in the transition-metal
dichalcogenides:

(1) We assume that only the octahedral sites, which
make themselves a two-dimensional triangular network, are
occupied. A possible low, but finite, occupation of the
tetrahedral sites is neglected.

(2) A two-dimensional model is applied on the basis
that no evidence for staging (i.e., long-range order along
the c axis) has been found either by X-ray[31,32] or by
neutron diffraction[16] techniques, although the appearance
of some imperfect ordering along the c axis has been suggested.[32]

(3) The picture[33] of Li ions residing in deep potential
wells centered on the lattice gas sites is supported by
measurements[23] giving an activation energy for Li diffusion
of about 0.3 eV, i.e., about 10 times larger than $k_B T_{room}$,
where $T_{room} = 300$ K.

(4). Small changes in the host due to the intercalation process appear mainly as changes in the strength of the interactions of the atoms, which can be incorporated in parameters of a rigid-lattice model.

We take the predominant interaction to be a Coulombic repulsion between two Li ions, strongly screened by the electrons in the host. The purely Coulombic interaction between two ions separated by the Li-Li distance $a = 3.46$ Å in $LiTiS_2$ is $e^2/a \approx 4.2$ eV. On the other hand, anticipating the results of Chapter IV, a reasonable fit of the incremental capacity curve of Li_xTiS_2 by a lattice gas model requires a nearest-neighbor repulsion of $5k_BT_{room} \approx 0.13$ eV, i.e., 30 times less than the purely Coulombic interaction. It is this strong screening that leads us to neglect interactions other than nearest-neighbor.

Intercalate atoms also interact through forces mediated by a strain field produced by dilation of the host structure during intercalation. Including elastic energy in a rigid-plate harmonic approximation, Dahn, Dahn and Haering[34] have obtained a good approximation for the incremental capacity of Li_xTiS_2, particularly for $x > 0.5$. Their model, however, uses three adjustable parameters to fit the experimental data and still fails on the peak at $x \approx 1/9$ by about 70%. A more accurate description of elastic contributions to the energy should certainly take into account the discreteness of the host lattice.

In the following chapters we concentrate on the application of the cluster-variation method[35] (CVM)--of which the mean-field approximation is a special case--to the two-dimensional triangular lattice gas as a model for Li_xTiS_2 and $Li_xTa_yTi_{1-y}S_2$. A complementary approach to the problem is the renormalization group method,[36] which has been applied by Berlinsky et al[37] to Li_xTiS_2. This approach leads to accurate order-disorder phase diagrams (within the limitations of the physical model, of course) and to the correct behavior of thermodynamic functions near critical points. Nevertheless, recent Monte-Carlo simulations[38] support our contention that the CVM approximation for a triangle as a basic cluster is better throughout most of the range of the thermodynamic parameters, where long-range fluctuations are not important.

REFERENCES: CHAPTER I

1. M.S. Whittingham, Science 192, 1126 (1976).

2. M.S. Whittingham and L.E. Ebert, in Physics and Chemistry
    of Materials with Layered Structures, F.A. Lévy, ed.,
    Vol. 6, p. 533 (Reidel, Dordrecht, Holland, 1979).

3. L.R. McCoy, in Special Topics in Electrochemistry,
    P. Rock, ed., p. 24 (Elsevier, New York, 1977).

4. D.W. Murphy and F.A. Trumbore, J. Crystal Growth 39,
    185 (1977).

5. F.R. Gamble and T.H. Geballe, in Treatise on Solid State
    Chemistry, N.B. Hannay, ed., Vol. 3, p. 84 (Plenum,
    New York, 1976).

6. M.S. Whittingham, Prog. Solid State Chem. 12, 41 (1978).

7. J.A. Wilson and A.D. Yoffe, Adv. Phys. 18, 193 (1969).

8. A.H. Thompson, Phys. Rev. Lett. 34, 520 (1975).

9. J. Rouxel, J. Physique Colloq. 38, C7 (1977).

10. J. Rouxel, Physica 99B, 3 (1980).

11. F. Hulliger, in Physics and Chemistry of Layered Compounds,
    F. Lévy, ed., Vol. 5 (Reidel, Dordrecht, Holland, 1977).

12. L.F. Mattheiss, Phys. Rev. B 8, 3719 (1973).

13. J.A. Wilson, Solid State Commun. 22, 551 (1977).

14. A.H. Thompson, F.R. Gamble and J.F. Revelli, Solid State
    Commun. 9, 981 (1971).

15. R. Schöllhorn, Physica 99B, 89 (1980).

16. J.R. Dahn, W.R. McKinnon, R.R. Haering, W.J.L. Buyers
    and B.M. Powell, Can. J. Phys. 58, 207 (1980).

17. R. Kleinberg, J. Phys. Chem. Solids 43, 3 (1982).

18. D.W. Murphy and J.N. Carides, J. Electrochem. Soc. 126,
    349 (1979).

19. R.B. Somono, V. Hadek and A. Rembaum, J. Chem. Phys. 58,
    697 (1973).

20. B.G. Silbernagel and M.S. Whittingham, J. Chem. Phys. 64,
    3670 (1976).

21. J.V. McCanny, J. Phys. C 12, 3263 (1979).

22. M.S. Whittingham, J. Electrochem. Soc. 123, 315 (1976).

23. B.G. Silbernagel, Solid State Commun. 17, 361 (1975).

24. A.H. Thompson, J. Electrochem. Soc. 126, 608 (1979).

25. A.H. Thompson, Phys. Rev. Lett. 40, 1511 (1978).

26. L.D. Landau and E.M. Lifschitz, Statistical Physics,
    Third Ed., Part 1, p. 342 (Pergamon, Oxford, 1980).

27. A.H. Thompson, Physica 99B, 100 (1980).

28. A.H. Thompson, K.R. Pisharody and R.F. Koehler, Jr.,
    Phys. Rev. Lett. 29, 163 (1972).

29. A.G. Khachaturyan, Phys. Status Solidi (b) 60, 9 (1973).

30. C.N. Yang and T.D. Lee, Phys. Rev. 84, 404 (1952). See
    also R.K. Pathria, Statistical Physics, pp. 397 ff.
    (Pergamon, Oxford, 1972).

31. T. Hibma, Physica 99B, 136 (1980).

32. J.R. Dahn and R.R. Haering, Solid State Commun. 40, 245
    (1981).

33. W.R. McKinnon and R.R. Haering, in <u>Modern Aspects of</u> <u>Electrochemistry</u>, J. O'M. Bockris and B.E. Conway, eds., to be published.

34. J.R. Dahn, D.C. Dahn and R.R. Haering, to be published.

35. R. Kikuchi, Phys. Rev. <u>81</u>, 988 (1951). See also the references in Chapter II of this dissertation.

36. See, e.g., S. Ma, <u>Modern Theory of Critical Phenomena</u> (Benjamin/Cummings, Reading, Mass., 1976).

37. A.J. Berlinsky, W.G. Unruh, W.R. McKinnon and R.R. Haering, Solid State Commun. <u>31</u>, 135 (1979).

38. W.R. McKinnon, Solid State Commun. <u>40</u>, 343 (1981).

Figure 1.1

Schematic representation of the band structure of 1T poly-
types of the MX_2 compounds. The Fermi level is indicated
for the cases of group-IVB and group-VB M atoms.
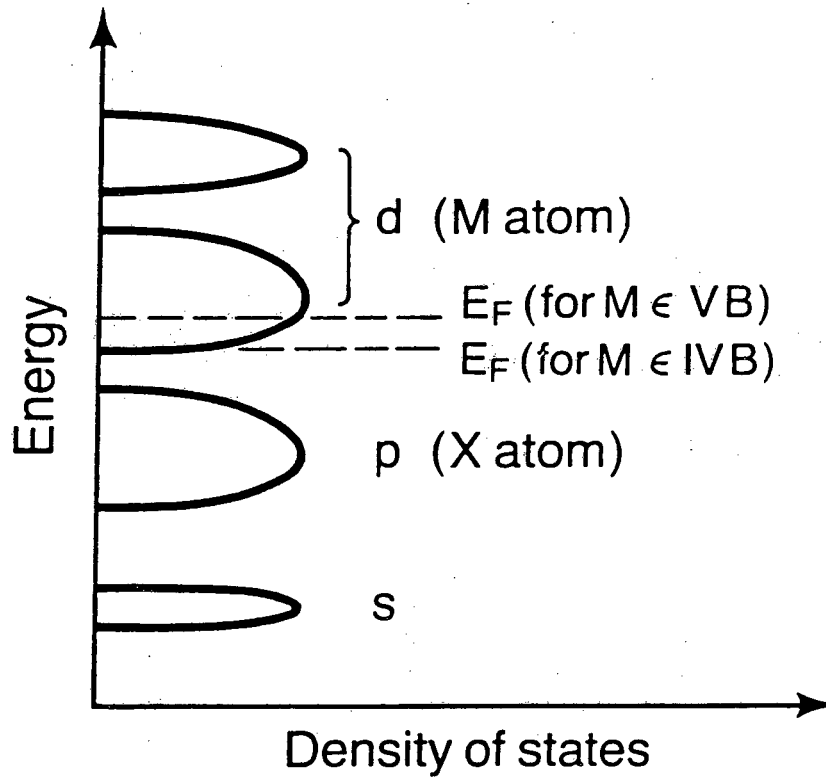
Figure 1.2

(a) Voltage-composition relation and (b) incremental
capacity curves for $Li_xTa_yTi_{1-y}S_2$, from Ref. 27.
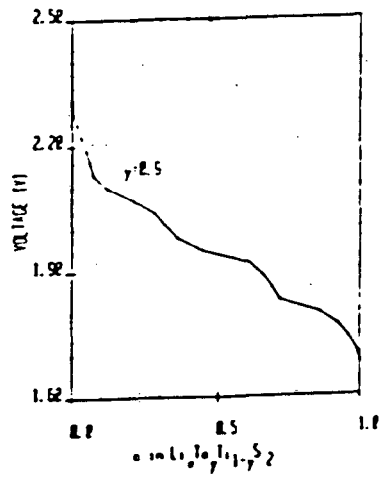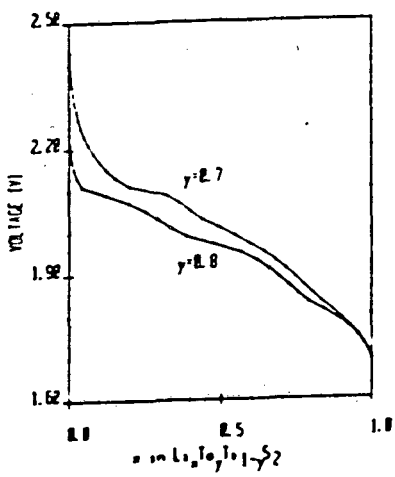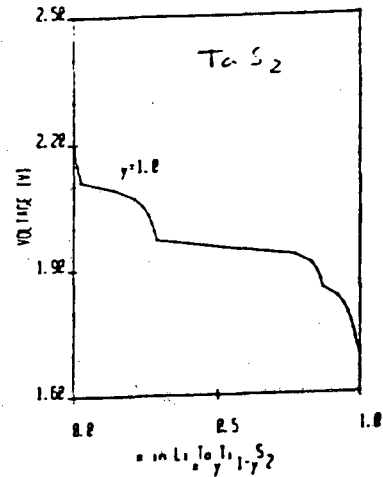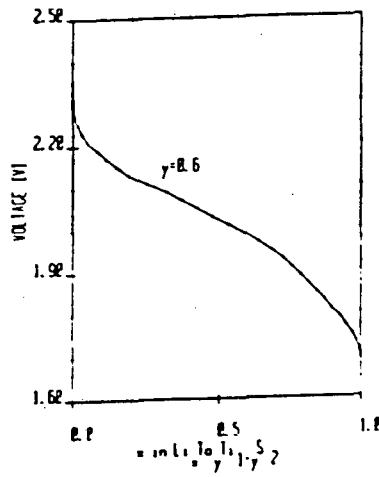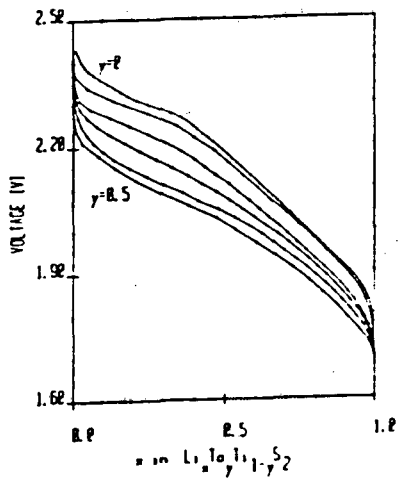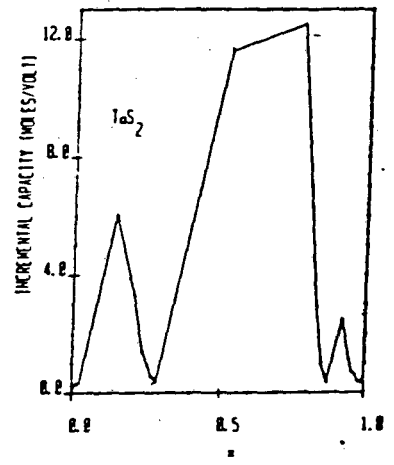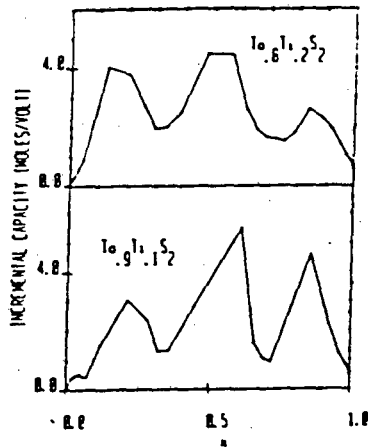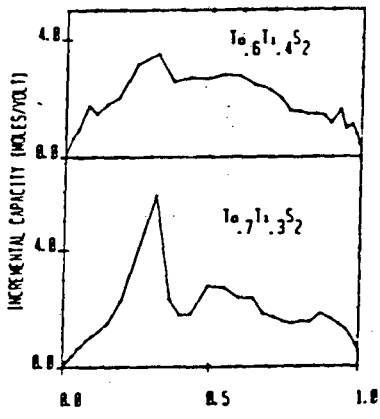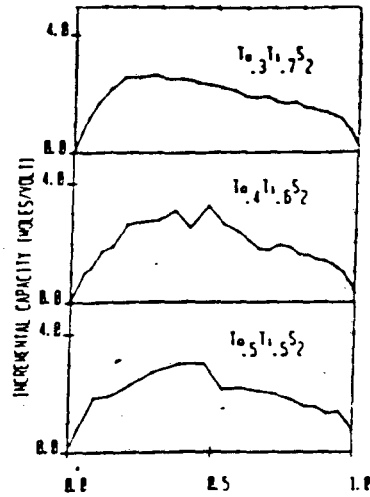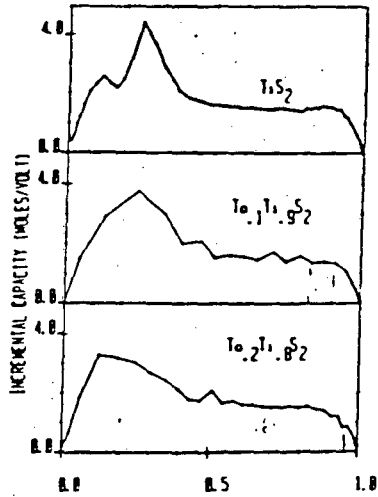
II. FORMULATION OF THE CLUSTER-VARIATION METHOD FOR THE LATTICE GAS MODEL

A. THE METHOD

Kikuchi[1] has developed the cluster-variation method (CVM) as a hierarchy of selfconsistent approximations for the combinatorial factors in the entropy of a lattice. The description of correlations between lattice sites is limited by the size of the chosen basic cluster, while long-range order can be introduced by dividing the lattice into a number of sublattices consistent with the ground state. The method can be equally applied to different types of solid solutions, e.g., metallic alloys, impurity solutions, and magnetic systems. In this chapter we concentrate on the formulation of CVM to the triangular lattice-gas problem.

We use the framework of the grand canonical ensemble: the chemical potential μ_1 and the temperature T of a given system are fixed by a particle reservoir which is also a heat bath. Each system of the ensemble is in one of the configurational states σ. By "configurational state" we mean a representative arrangement of $Nx(\sigma)$ particles and $N[1-x(\sigma)]$ vacancies in the lattice gas with a total energy $E(\sigma)$. The number of such equivalent arrangements is the statistical weight $g(\sigma)$. The following argument is found, e.g., in de Fontaine's review article[2] in the context of the canonical ensemble.

The configurational grand partition function is

$$Z = \sum_{\sigma} g(\sigma)\, e^{[Nx(\sigma)\mu_1 - E(\sigma)]/k_B T} \quad . \tag{2.1}$$

In the thermodynamic limit ($N \to \infty$), fluctuations about the most probable state are neglected and the sum in Eq. (2.1) is replaced by its maximum term

$$Z \cong \underset{\sigma}{\text{Max}}\; g(\sigma) e^{[Nx(\sigma)\mu_1 - E(\sigma)]/k_B T} \tag{2.2}$$

$$\equiv e^{-\Omega_{eq}/k_B T} \quad .$$

This last equivalence defines the equilibrium grand potential Ω_{eq} as the minimum of the generalized grand potential $\Omega(\sigma)$ among all possible states σ, where

$$\Omega(\sigma) = E(\sigma) - TS(\sigma) - Nx(\sigma)\mu_1 \quad , \tag{2.3}$$

and

$$S(\sigma) = k_B \ln g(\sigma) \tag{2.4}$$

is the configurational entropy.

Once Ω_{eq} is known, as a function of μ_1 and T, the thermodynamic properties of the system follow from the fundamental equality

$$d\Omega_{eq} = -S_{eq}\,dT - Nx_{eq}\,d\mu_1 \quad , \tag{2.5}$$

which assumes no variation of the total area of the lattice

gas. To obtain Ω_{eq} we would have, in principle, to specify all configurational states of the whole lattice. The CVM scheme consists of replacing this impossible task by a description of probabilities of the configurational states of a chosen basic cluster of sites. The main problem is then reduced to finding a suitable expression for $g(\sigma)$, where σ now stands for a given set of probabilities of the basic cluster. The CVM formulations of $g(\sigma)$ take into account the contributions of sites outside the basic cluster only in an approximate manner. In general the approximation becomes more accurate when a larger basic cluster is chosen,[3,4] with a cost to be paid, however, that the expression for $g(\sigma)$ rapidly increases in complexity.

Sanchez and de Fontaine[5] have devised a scheme which takes correlation functions (from which the cluster probabilities can be obtained by a "cluster algebra") as the basic minimization parameters. The original basic-cluster configurations, however, are better suited for the minimization of $\Omega(\sigma)$ through the use of Kikuchi's[6] "natural iteration" method. This is applied in Chapter IV, with the triangle taken as basic cluster. In the following section we derive the CVM expressions for the statistical weight $g(\sigma)$, and hence the grand potential $\Omega(\sigma)$, with the single site and with the nearest-neighbor triangle as basic clusters.

The pair approximation is equivalent to the Bethe-Peierls[7] method and has been applied to the triangular

lattice with repulsive nearest-neighbor and attractive second-nearest-neighbor interactions by Campbell and Schick.[8] Because of its "one-dimensional" characteristics, however, this model leads to paradoxical results, like negative entropies close to the concentration $x = 1/2$ at low temperatures. Another failure, apparent in all closed-packed lattices, is that the Bethe-Peierls method gives wrong results for the energy at zero temperature: the probability of existence of nearest-neighbor pairs of particles is zero for $x \leq 1/2$, while, as discussed in Chapter III, the correct result is finite for $x > 1/3$. We therefore choose not to apply the pair approximation to the present problem, although an expression for $g(\sigma)$ in the pair approximation is obtained in the next section as a step toward the triangle approximation.

    B.   EXPRESSIONS FOR THE GRAND POTENTIAL IN DIFFERENT
         APPROXIMATIONS

As mentioned in the previous section, long-range order can be described in a lattice through its representation in terms of appropriate sublattices. We say that long-range order exists when one of the sublattices is preferentially occupied.

The simplest case of a CVM approximation, when a single site is taken as the basic cluster, is equivalent to a mean-field (or Bragg-Williams[9]) model. We refer to the single-site approximation as the generalized mean-field model when a representation in terms of sublattices is intro-

duced. Otherwise, we call it the regular mean-field model. Both approximations neglect all types of short-range correlations between sites.

In what follows we consider only the nearest-neighbor repulsion U, and in the case of the triangle approximation a three-particle interaction is added. The temperature T, the chemical potential μ_1, the total energy E, the grand potential Ω, and the entropy S are hereafter expressed in the dimensionless forms

$$\tau = \frac{k_B T}{U} \ , \ \mu = \frac{\mu_1}{U} \ , \ \epsilon = \frac{E}{NU} \ , \ \omega = \frac{\Omega}{NU} \ ; \tag{2.6}$$

and

$$s = \frac{S}{Nk_B} = \frac{1}{N} \ln g \ , \tag{2.7}$$

where we have dropped the argument σ for simplicity. We can then write Eq. (2.3) as

$$\omega = \epsilon - \tau s - \mu x \ . \tag{2.8}$$

1. Regular mean-field model

In the simplest approximation, the set σ of configurational probabilities is limited to the fractional occupation x of the lattice. The statistical weight g is simply the number of different ways we can arrange Nx particles and N(1-x) vacancies among the N lattice sites, i.e.

$$g = \frac{N!}{(Nx)![N(1-x)]!} \cdot \tag{2.9}$$

The mean-field approximation for the energy consists of taking the mean occupation $\underline{x}$ of the lattice as the mean distribution of atoms on the nearest-neighbor sites about a given occupied site. We then have

$$\epsilon = 3x^2 \quad , \tag{2.10}$$

which makes use of the fact that there are three nearest-neighbor bonds per site in the triangular lattice. The application of Stirling's approximation to Eq. (2.7) yields for the reduced grand potential

$$\omega = 3x^2 + \tau[x \ln x + (1-x) \ln(1-x)] - \mu x \quad . \tag{2.11}$$

This grand potential can be immediately minimized with respect to $\underline{x}$. The minimization condition

$$\frac{\partial \omega}{\partial x} = 0 \quad , \tag{2.12}$$

yields for the chemical potential

$$\mu = 6x + \tau \ln \frac{x}{1-x} \quad . \tag{2.13}$$

This result is discussed in Chapter III.

2. Generalized mean-field model

We now introduce a sublattice representation for the description of long-range order. As illustrated in Fig. 2.1, the triangular lattice is divided into three interpenetrating sublattices, α, β, and γ, such that any site in one of them, say α, has three nearest neighbors in each of the other two sublattices, β and γ. This representation can be justified by the work of Kanamori and Kaburagi,[10] who found the ground-state structures for the triangular lattice gas with various pairwise interactions. In our notation, for nearest-neighbor repulsions only, we have the following equilibrium configurations: for $x = 1/3$ the α sublattice full, $n_\alpha = 1$, with empty β and γ sublattices, $n_\beta = n_\gamma = 0$; for $x = 2/3$ the α and β sublattices full, $n_\alpha = n_\beta = 1$, and the γ sublattice empty, $n_\gamma = 0$. We define by n_ν ($\nu = \alpha, \beta, \gamma$) the probability that a lattice site of sublattice ν is occupied by an atom. We thus have

$$x = \frac{1}{3} (n_\alpha + n_\beta + n_\gamma) \quad . \tag{2.14}$$

The statistical weight g is taken to be the product of the mean-field statistical weights of the three sublattices:

$$g = \prod_\nu \frac{(N/3)!}{(Nn_\nu/3)![N(1-n_\nu)/3]!} \tag{2.15}$$

In the mean-field model, the interaction energy is approx-

imated by

$$\varepsilon = n_\alpha n_\beta + n_\beta n_\gamma + n_\gamma n_\alpha \quad . \tag{2.16}$$

The reduced grand potential now becomes

$$\omega = n_\alpha n_\beta + n_\beta n_\gamma + n_\gamma n_\alpha$$

$$+ \frac{\tau}{3} \sum_\nu [n_\nu \ln n_\nu + (1-n_\nu) \ln(1-n_\nu)] \tag{2.17}$$

$$- \frac{\mu}{3} (n_\alpha + n_\beta + n_\gamma) \quad .$$

The minimization of ω with respect to n_α, n_β and n_γ is discussed in Chapter III.

3. Triangle approximation

The triangle approximation includes nearest-neighbor correlations between sites. In addition, it allows in a natural way the introduction of three-particle interactions, whose physical meaning is discussed in Chapter IV.

We define as our basic cluster a closed triangle containing nearest-neighbor points belonging to the three different sublattice of Fig. 2.1. To each lattice site we associate a number $\underline{i}$ such that $i = 0$ if the site is empty and $i = 1$ if the site is occupied. Accordingly, we define the point probabilities x_i^ν for the $\underline{i}$ state of a point in the sublattice ν ($\nu = \alpha$, β or γ). In the notation of the pre-

ceding sub-section (II-B-2), $x_1^\nu = n_\nu$. The probability for an $\underline{i} - \underline{j}$ bond (where i, j = 0 or 1) between nearest-neighbor sites on the sublattices ν and ν' is denoted by $y_{ij}^{\nu\nu'}$. Finally the probability for an $\underline{i} - \underline{j} - \underline{k}$ configuration on an equilateral nearest-neighbor triangle containing points on the sublattices α, β and γ, in this order, is denoted by z_{ijk}. The following relations hold between the configuration probabilities for the different clusters:

$$\sum_{ijk} z_{ijk} = 1 \qquad (2.18a)$$

$$y_{ij}^{\alpha\beta} = \sum_k z_{ijk} \; ; \qquad y_{jk}^{\beta\gamma} = \sum_i z_{ijk} \; ; \qquad y_{ki}^{\gamma\alpha} = \sum_j z_{ijk} \; ; \quad (2.18b)$$

$$x_i^\alpha = \sum_{jk} z_{ijk} \; ; \qquad x_j^\beta = \sum_{ik} z_{ijk} \; ; \qquad x_k^\gamma = \sum_{ij} z_{ijk} \; . \quad (2.18c)$$

Various schemes can be used for obtaining CVM approximations for the statistical weight in the expression for the entropy. Here we use the "pseudo-assembly method",[11] which gives the same results as the original[1] CVM formulation. In the following, for the sake of clarity, we temporarily drop the sublattice indices.

Let us first reconsider the single-site approximation. We can rewrite Eq. (2.9) as

$$g_{(1)} = \frac{N!}{\{site\}} \equiv Q_{(1)}^1 \quad , \qquad (2.19)$$

where we define the CVM symbol

$$\{\text{site}\} \equiv \prod_i (Nx_i)! \tag{2.20}$$

Here $x_0 = 1 - x$ and $x_1 = x$ are the probabilities for finding a vacancy or an atom, respectively, on a given lattice site. The subscript of g and Q is the number of sites in the cluster under consideration. The meaning of the superscript, which can also be interpreted as an exponent, will become clear in the following discussion.

Given the pair probabilities y_{ij}, let us now consider a general distribution of pair configurations on the 3N nearest-neighbor bonds of the lattice. The number of such arrangements in a triangular lattice is

$$Q_{(2)}^3 = \frac{(3N)!}{\prod_{ij} (3Ny_{ij})!}$$

$$= \left[\frac{N!}{\{\text{pair}\}} \right]^3 , \tag{2.21}$$

where

$$\{\text{pair}\} \equiv \prod_{ij} (Ny_{ij})! \tag{2.22}$$

The last equality in Eq. (2.21) follows trivially from Stirling's approximation.

As illustrated in Fig. 2.2(a), the number $Q_{(2)}^3$ includes

a high proportion (very close to unity) of "incorrect" distributions, where particles and vacancies are simultaneously associated with the same site. We now have to estimate a correction factor $\Gamma_{(2)}$ ($\ll 1$) such that the statistical weight is

$$g_{(2)} \approx \Gamma_{(2)} \, Q_{(2)}^3 \quad . \tag{2.23}$$

To do this we consider the "pseudo-assembly" of Fig. 2.2(b), where six particles or vacancies are assigned to each site. There are $Q_{(1)}^6$ possible arrangements on the 6N sites of this pseudo-assembly. Of these, the number $Q_{(1)}^1$, given by Eq. (2.19), are "correct" arrangements, in the sense that no particles and vacancies are simultaneously assigned to a given site, as illustrated in Fig. 2.2(c). Thus we have a proportion $Q_{(1)}^1 / Q_{(1)}^6 = Q_{(1)}^{-5}$ of "correct" arrangements in the pseudo-assembly.

The fundamental conceptual step in the CVM approximation is to take the proportion of "correct" arrangements in the pseudo-assembly as the right proportion of "correct" arrangements for the distribution of the basic-cluster configurations. In the pair approximation, this amounts to take

$$\Gamma_{(2)} = Q_{(1)}^{-5} \quad , \tag{2.24}$$

and

$$g_{(2)} = Q_{(1)}^{-5} \, Q_{(2)}^3$$

$$= \frac{\{site\}^5}{(N!)^2 \{pair\}^3} \quad . \tag{2.25}$$

Let us now consider a general distribution of triangle configurations on the 2N nearest-neighbor triangles of the lattice, as illustrated in Fig. 2.3(a). The number of such arrangments is

$$Q_{(3)}^2 = \left[\frac{N!}{\{triangle\}} \right]^2 \quad , \tag{2.26}$$

where

$$\{triangle\} = \prod_{ijk} (Nw_{ijk})! \tag{2.27}$$

Here w_{ijk} is the i-j-k configuration triangle probability without sublattice considerations, as opposed to the z_{ijk} of Eq. (2.18). We now consider the pseudo-assembly of Fig. 2.3(b), where two pair configurations are assigned to each lattice bond. The number of "correct" arrangements of these pairs, Fig. 2.3(c), is approximated by Eq. (2.25), while the number of total arrangements is

$$h \approx Q_{(2)}^6 \frac{Q_{(1)}^6}{Q_{(1)}^{12}} \quad . \tag{2.28}$$

Here $Q_{(2)}^6$ is the number of ways of distributing 6N pair configurations (3N double pairs) of any kind on the lattice bonds, while $Q_{(1)}^6/Q_{(1)}^{12} = Q_{(1)}^{-6}$ is the correction factor for obtaining only configurations of the type of Fig. 2.3(b), where pairs on neighboring bonds that have been split from the same triangle converge to a well defined (either a particle or a vacancy) "pair site". (Good distributions in this sense have six well

defined "pair sites" out of twelve possible "pair sites" per lattice site.) We thus take the correction factor for the triangle cluster

$$\Gamma_{(3)} = g_{(2)}/h$$

$$= Q_{(1)}^{1} \, Q_{(2)}^{-3} \quad .$$

(2.29)

The CVM approximation for the statistical weight is then

$$g_{(3)} = \Gamma_{(3)} \, Q_{(3)}^{2}$$

$$= \frac{\{pair\}^3}{\{triangle\}^2\{site\}} \quad .$$

(2.30)

We now return to the three-sublattice representation. A little reflection shows that the three lattice triangles that differ by a cyclic combination of the lattice indices ought to contribute equally to the statistical weight. We thus replace

$$\{site\} \leftarrow \prod_{i} \prod_{\nu} \left(\frac{N}{3}x_i^{\nu}\right)! \tag{2.31a}$$

$$\{pair\}^3 \leftarrow \prod_{ij} \left(Ny_{ij}^{\alpha\beta}\right)! \left(Ny_{ij}^{\beta\gamma}\right)! \left(Ny_{ij}^{\gamma\alpha}\right)! \tag{2.31b}$$

$$\{triangle\}^2 \leftarrow \prod_{ijk} \left(2Nz_{ijk}\right)! \tag{2.31c}$$

The statistical weight is then written as

$$g = \frac{\prod\limits_{ij} \left(Ny_{ij}^{\alpha\beta}\right)! \; \left(Ny_{ij}^{\beta\gamma}\right)! \; \left(Ny_{ij}^{\gamma\alpha}\right)!}{\prod\limits_{ijk} \left(2Nz_{ijk}\right)! \; \prod\limits_{\nu} \prod\limits_{i} \left(\frac{N}{3}x_i^{\nu}\right)!} \quad . \qquad (2.32)$$

In the triangle approximation the reduced interaction energy is

$$\epsilon = y_{11}^{\alpha\beta} + y_{11}^{\beta\gamma} + y_{11}^{\gamma\alpha} + 2\phi z_{111} \quad , \qquad (2.33)$$

where the value $U\phi$ was added for each fully-occupied nearest-neighbor triangle of sites. The reduced grand potential can then be expressed as

$$\omega = y_{11}^{\alpha\beta} + y_{11}^{\beta\gamma} + y_{11}^{\gamma\alpha} + 2\phi \; z_{111}$$

$$+\tau \left\{ 2 \sum\limits_{ijk} L(z_{ijk}) \right.$$

$$- \sum\limits_{ij} L(y_{ij}^{\alpha\beta}) - \sum\limits_{jk} L(y_{jk}^{\beta\gamma}) - \sum\limits_{ki} L(y_{ki}^{\gamma\alpha}) \qquad (2.34)$$

$$+ 1/3 \left[\sum\limits_{i} L(x_i^{\alpha}) + \sum\limits_{j} L(x_j^{\beta}) + \sum\limits_{k} L(x_k^{\gamma}) \right] \right\}$$

$$- \frac{1}{3}\mu \; (x_1^{\alpha} + x_1^{\beta} + x_1^{\gamma}) \quad ,$$

where the operator L, defined as

$$L(u) = u(\ln u - 1) \quad , \qquad (2.35)$$

results from using Stirling's approximation in the expression
for the entropy. The eight triangle configuration probab-
ilities z_{ijk} are taken as independent variables for the
minimization of ω, for given μ, τ and ϕ. This is examined in
Chapter IV.

REFERENCES: CHAPTER II

1. R. Kikuchi, Phys. Rev. 81, 988 (1951); J. Physique Colloq.
    38, C7 (1977).

2. D. de Fontaine, Solid State Phys. 34, 73 (1979).

3. R. Kikuchi and S.G. Brush, J. Chem. Phys. 47, 195 (1967).

4. J.K. McCoy, R. Kikuchi and H. Sato, Physica 109A, 445
    (1981).

5. J.M. Sanchez and D. de Fontaine, Phys. Rev. B 17, 2926
    (1978).

6. R. Kikuchi, J. Chem. Phys. 60, 1071 (1974).

7. H.A. Bethe, Proc. R. Soc. A 150, 552 (1935); R. Peierls,
    Proc. Cambr. Phil. Soc. 32, 477 (1936).

8. C.E. Campbell and M. Schick, Phys. Rev. A 5, 1919 (1972).

9. W.L. Bragg and E.J. Williams, Proc. Roy. Soc. (London)
    A145, 699 (1934). See also C. Barrett and T.B. Massalski,
    Structure of Metals, pp. 284 ff. (3rd ed., McGraw-Hill,
    New York, 1966).

10. M. Kaburagi and J. Kanamori, Japan J. Appl. Phys. Suppl.
     2, Pt. 2 (Proc. 2nd Intl. Conf. on Solid Surfaces, Kyoto),
     145 (1974); J. Phys. Soc. Japan, 44, 718 (1978).

11. M. Kurata, R. Kikichi and T. Watari, J. Chem. Phys. 21,
     434 (1953). See also J.M. Ziman, Models of Disorder,
     sec. 5.4 (Cambridge University, Cambridge, 1979).

Figure 2.1

Representation of the triangular lattice with its three interprenetrating sublattices.
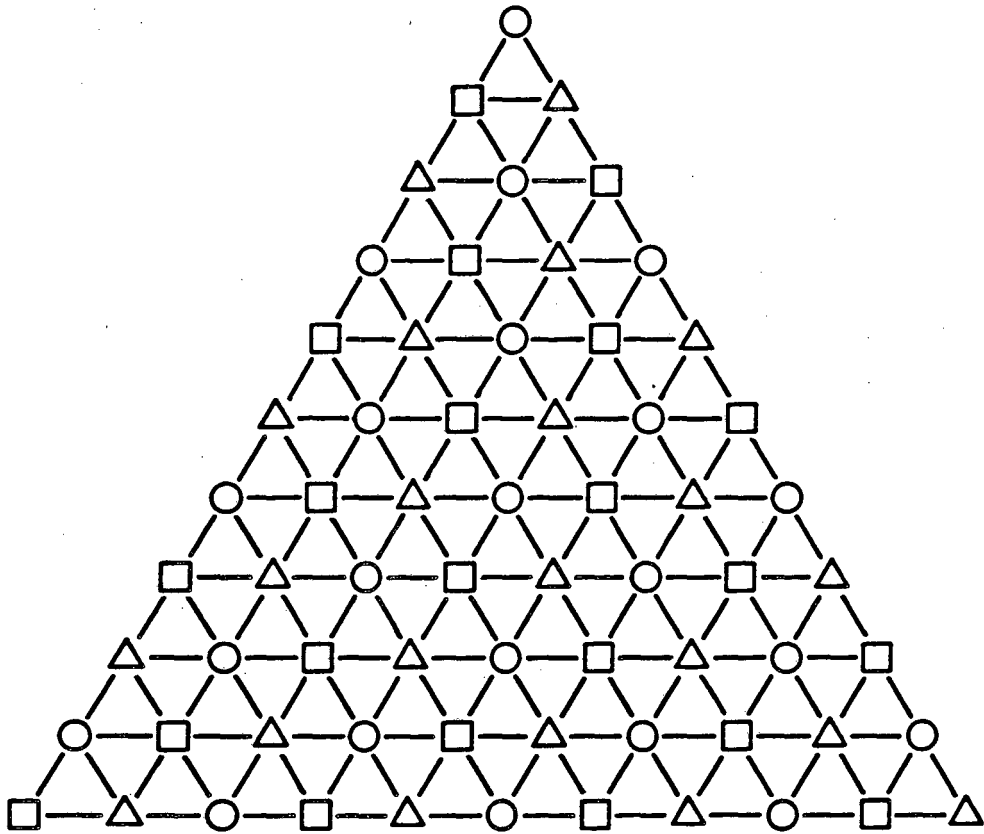
Figure 2.2

The pseudo-assembly method for the pair approximation:
(a) general distribution of pair configurations on lattice
bonds; (b) pseudo-assembly of particles and vacancies on
sites; (c) "correct" distribution of pairs.
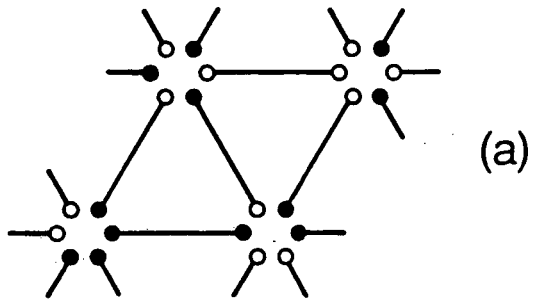
(a)

(b)
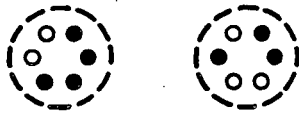
(c)
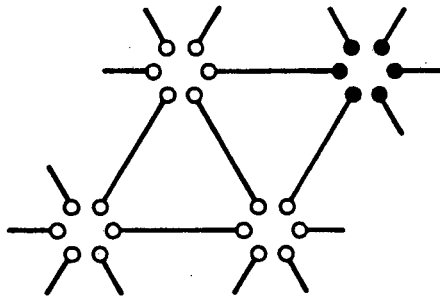
Figure 2.3

The pseudo-assembly method for the triangle approximation:
(a) general distribution of triangle configurations on the
lattice triangles; (b) pseudo-assembly of pair configura-
tions on lattice bonds; (c) "correct" distribution of triangles.

(a)

(b)

(c)
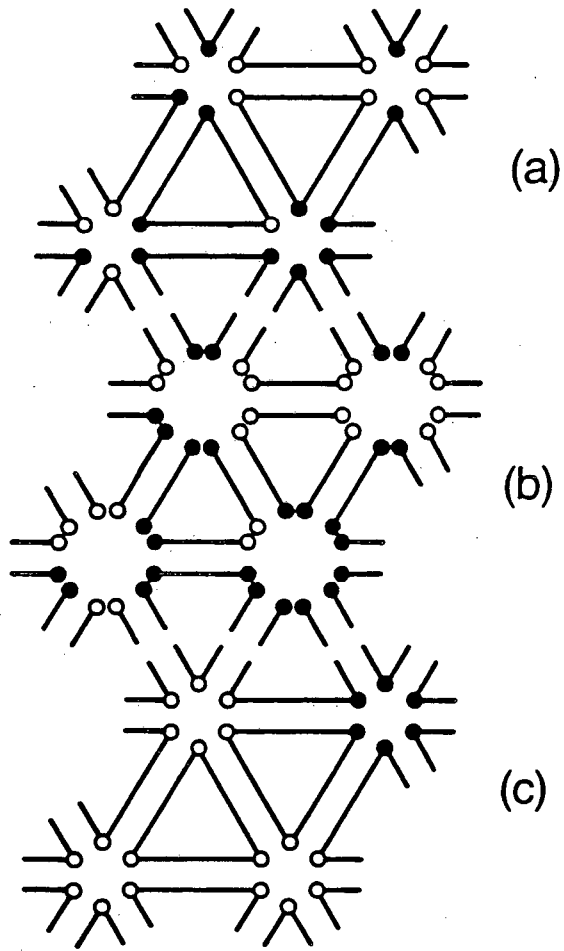
III. MEAN-FIELD THEORY FOR $Li_x TiS_2$

A. CALCULATION

In this chapter we develop in detail the three-sublattice mean-field model of the triangular lattice gas introduced in sub-section II-B-2. The results are compared with the experimental data of Thompson[1] for $Li_x TiS_2$. Features like maxima and minima of the incremental capacity curve are interpreted in terms of the behavior of the variables of our model.

We start with the reduced grand potential of Eq. (2.17), which we rewrite as

$$\omega = \frac{9}{2} x^2 + \sum_\nu y(n_\nu) \quad , \qquad (3.1)$$

where

$$y(n_\nu) = -\frac{1}{2}(n_\nu)^2 + \frac{\tau}{3}[n_\nu \ln n_\nu$$

$$\qquad (3.2)$$

$$+ (1-n_\nu) \ln (1-n_\nu)] - \frac{1}{3} \mu n_\nu \quad .$$

The notation is that of Chapter II. Nearest-neighbor pairwise repulsions are the only contribution to the energy. For given μ and τ, at the equilibrium state we must have

$$\frac{\partial \omega}{\partial n_\nu} = 3x + y'(n_\nu) = 0 \qquad (3.3)$$

where

$$y'(n_\nu) = -n_\nu + \frac{\tau}{3} \ln \frac{n_\nu}{1-n_\nu} - \frac{\mu}{3} \quad . \qquad (3.4)$$

Eqs. (3.3) and (3.4) can be solved by assigning values to

$$\lambda = -3x + \frac{\mu}{3} \qquad\qquad (3.5)$$

and solving the equation

$$g(n_\nu) \equiv -n_\nu + \frac{\tau}{3} \ln \frac{n_\nu}{1-n_\nu} = \lambda \qquad\qquad (3.6)$$

by a Newton-Raphson procedure.[2]

For $\tau < \tau_c = 3/4$, Eq. (3.6) has three different roots between 0 and 1 whenever λ is such that $g(u_+) < \lambda < g(u_-)$, where

$$u_\pm = \frac{1}{2} \pm \left(\frac{1}{4} - \frac{\tau}{3}\right)^{1/2} \qquad . \qquad\qquad (3.7)$$

The three roots, which we call u_1, u_2 and u_3, can be assigned in ten different ways to the three sublattice probabilities n_α, n_β and n_γ. For instance, we can have the triplets

$$\{n_\alpha, n_\beta, n_\gamma\} = \{u_1, u_1, u_1\} \quad ,$$
$$\{u_1, u_1, u_2\} \quad , \text{ etc.} \qquad\qquad (3.8)$$

Comparison of the resulting grand potentials as functions of the chemical potential for the ten triplets leads to the phase diagram of Fig. 3.1. The complete phase diagram displays a mirror symmetry about the line $x = 1/2$. This is a consequence of the pairwise, concentration-independent nature of the assumed interactions, which leads to a particle-vacancy

symmetry. As noted by Van Baal,[3] this is independent of the order of the approximation. We define the different regions in the phase diagram as: the disordered phase (3), where $n_\alpha = n_\beta = n_\gamma$; the ordered phases (12), where $n_\alpha > n_\beta = n_\gamma$, (21), where $n_\alpha = n_\beta > n_\gamma$, and (111), where $n_\alpha > n_\beta > n_\gamma$. The (21) phase is the mirror image of phase (12) about $x = 1/2$.

In the present approximation the particle-vacancy symmetry is translated by the relations

$$n_\alpha(x = x_0) = 1 - n_\gamma(x = 1 - x_0) \tag{3.9}$$

and

$$n_\beta(x = x_0) = 1 - n_\beta(x = 1 - x_0) \quad . \tag{3.10}$$

It can then be readily shown the

$$\mu(x = x_0) = 6 - \mu(x = 1 - x_0) \tag{3.11}$$

and

$$\left(\frac{\partial x}{\partial \mu}\right)_{x = x_0} = \left(\frac{\partial x}{\partial \mu}\right)_{x = 1 - x_0} \quad . \tag{3.12}$$

An alternative method for solving the lattice-gas problem is to consider the concentration $\underline{x}$ as the thermodynamic parameter instead of the (reduced) chemical potential μ. Because of the constraint of Eq. (2.14), only two of the three sub-lattice probabilities are independent variational parameters for the minimization of the reduced free energy

$$f \equiv \frac{F}{NU} = \varepsilon - \tau s \quad . \tag{3.13}$$

The reduced chemical potential μ is then given by the derivative $(\partial f / \partial x)$. This procedure is in fact more convenient for the phases (3), (12) and (21), where at least two of the sublattice probabilities are taken to be equal. This leads to a minimization equation of only one variable.

B. RESULTS AND DISCUSSION

A physical insight into the meaning of the different phases may be gained by considering the behavior of the lattice gas at $T = 0$. The reduced free energy is then given by the broken line in Fig. 3.2. If we increase the concentration of occupied sites, only the α sublattice is being filled in the interval $0 < x < 1/3$, where $n_\alpha = 3x$, $n_\beta = n_\gamma = 0$. The β sublattice is filled in the interval $1/3 < x < 2/3$, where $n_\alpha = 1$, $n_\beta = 3x - 1$, $n_\gamma = 0$. Finally the γ sublattice is filled in the interval $2/3 < x < 1$, where $n_\alpha = n_\beta = 1$, $n_\gamma = 3x - 2$. Thus at $T = 0$, for $1/3 < x < 2/3$ the system is in the (111) phase; otherwise it is in the (12) or the (21) phase. As the temperature increases, the entropy term in the free energy reduces the range of existence of the (111) phase and induces the appearance of a completely disordered phase (3), which emerges from the $x = 0$ and $x = 1$ extremes of the allowed range of concentrations and occupies the whole concentration range when the reduced temperature exceeds the critical value $\tau_c = 3/4$.

The zero-temperature picture discussed above is only valid in the present mean-field approximation, where an

ordered phase is artificially required to avoid nearest-
neighbor pairs. In the next chapter, however, we show
that short-range correlations can actually lead to long-
range disorder even at T = 0.

The phases (3) and (12) or (21) are connected by a
first-order transition; the phases (12) or (21) and (111)
are connected by a second-order phase transition. For a
given $\tau < \tau_c$ there is a small interval of values of $\underline{x}$ in
each half of the phase diagram where the phases (3) and (12)
or (21) coexist in a heterogeneous mixture. In this region
$\underline{f}$ is a linear function of $\underline{x}$, defined by the common tangent
to the $\underline{f}$-versus-$\underline{x}$ curves for the two coexisting phases, and
both the chemical potential and the grand potential are con-
stant. The incremental capacity $(-\partial x/\partial V)$ is given in our
dimensionless units by $(\partial x/\partial \mu)$. At $\tau = 0$ this function is
zero at x = 0, 1/3, 2/3, 1, and infinite otherwise. It is
more convenient to use the function $(\tau \cdot \partial x/\partial \mu)$ which has
slope ± 1 at x = 0, 1 for any value of τ. This function is
plotted in Fig. 3.3 for several temperatures. For $\tau > \tau_c$,
we have the regular mean-field result from Eq. (2.13),

$$\tau \frac{\partial x}{\partial \mu} = \left[\frac{6}{\tau} + \frac{1}{x(1-x)} \right]^{-1} , \qquad (3.14)$$

i.e. a smooth, structureless curve.

Our incremental capacity diverges over the small inter-
vals of $\underline{x}$ where the phases (3) and (12) or (21) coexist. On

the other hand, no singularities occur at values of the concentration where ordered arrangements of the particles are expected. On the contrary, at small values of τ, there are minima of $(\partial x/\partial \mu)$ near $x = 1/3$ and $2/3$, where ordered configurations exist. This is intuitively expected: a significant change in the chemical potential should be required to modify the structure at those concentrations. We thus confirm the conclusions of Berlinsky et al[4] concerning the meaning of minima and maxima of the incremental capacity. In our model, however, this function diverges over small x-intervals, rather than only at isolated points.

C. CONCLUSIONS

In this chapter we have studied the order-disorder phase diagram for a three-sublattice representation of a triangular lattice gas with a nearest-neighbor repulsive interaction. A single-site approximation has been used as the first step towards a more sophisticated triangle cluster approximation, discussed in Chapter IV. In spite of its simplicity the approximation used here can account qualititavely for the experimental features in the incremental capacity of systems like Li_xTiS_2.

We have found that minima of the incremental capacity occur at the concentrations where ordered structures form and divergences are associated with the coexistence of two phases (one ordered and the other one disordered) and do not necessarily occur at concentrations that can be expressed

as rational numbers of small denominator. Smooth maxima
(e.g. at $x = 1/2$ at any temperature and at $x \simeq 1/2$ and
$x \simeq 5/6$ at very low temperatures in our model) can appear
at concentrations that are not structurally meaningful and
are not related to ordering effects.

REFERENCES: CHAPTER III

1.   Chapter I, refs. 24, 25.

2.   See, e.g., G. Dahlquist and Å. Björck, <u>Numerical Methods</u>,
     pp. 222ff. (Prentice-Hall, Englewood Cliffs, NJ, 1974).

3.   C.M. Van Baal, Physica <u>64</u>, 571 (1973).

4.   Chapter I, ref. 37.

Figure 3.1

Phase diagram for the triangular lattice gas in the (x, τ) plane. The dashed line is the locus of equal free energies for the (3) and (12) phases.
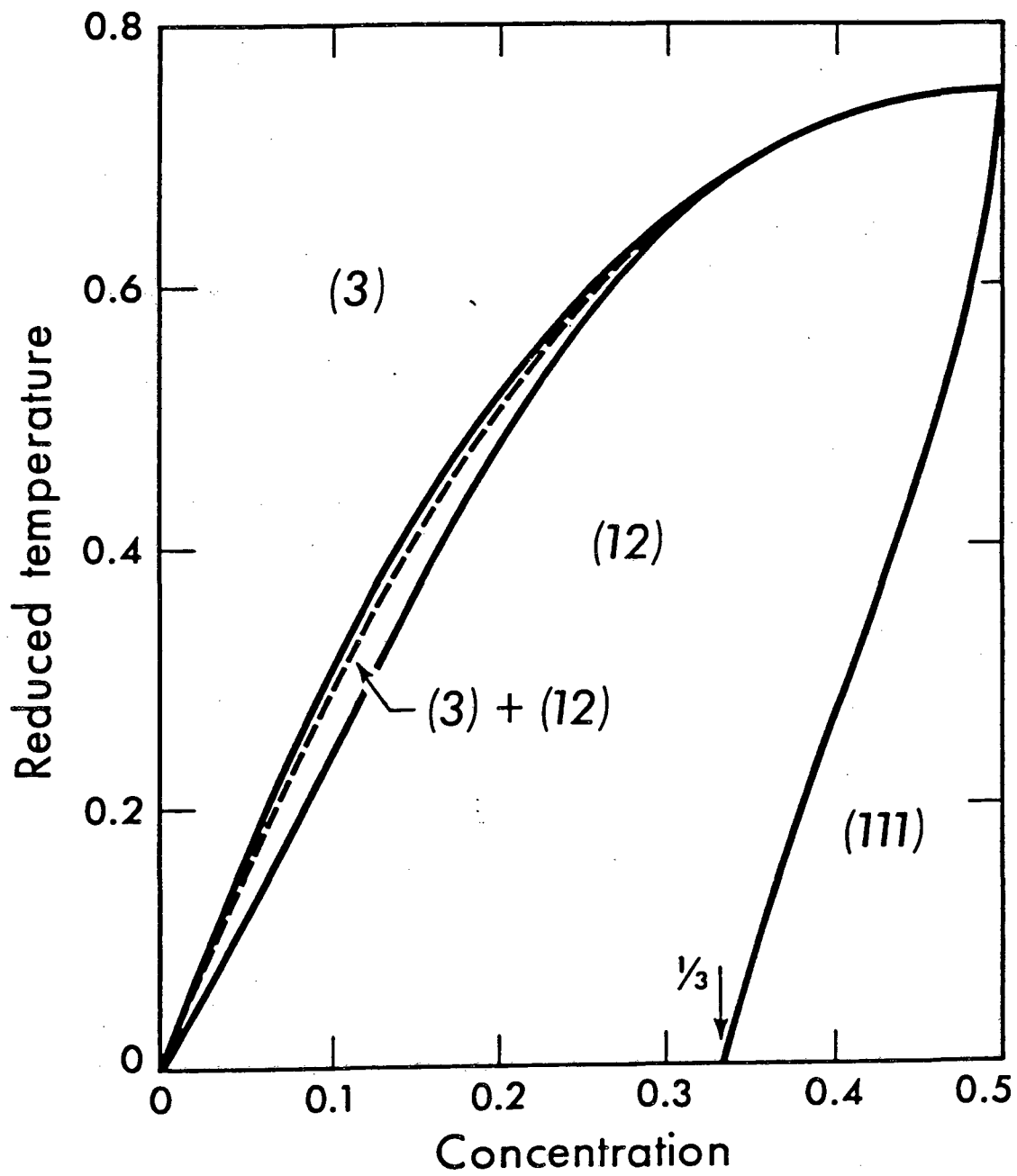
Figure 3.2

Reduced energy $\underline{f}$ as a function of concentration $\underline{x}$ for $\tau = 0$.
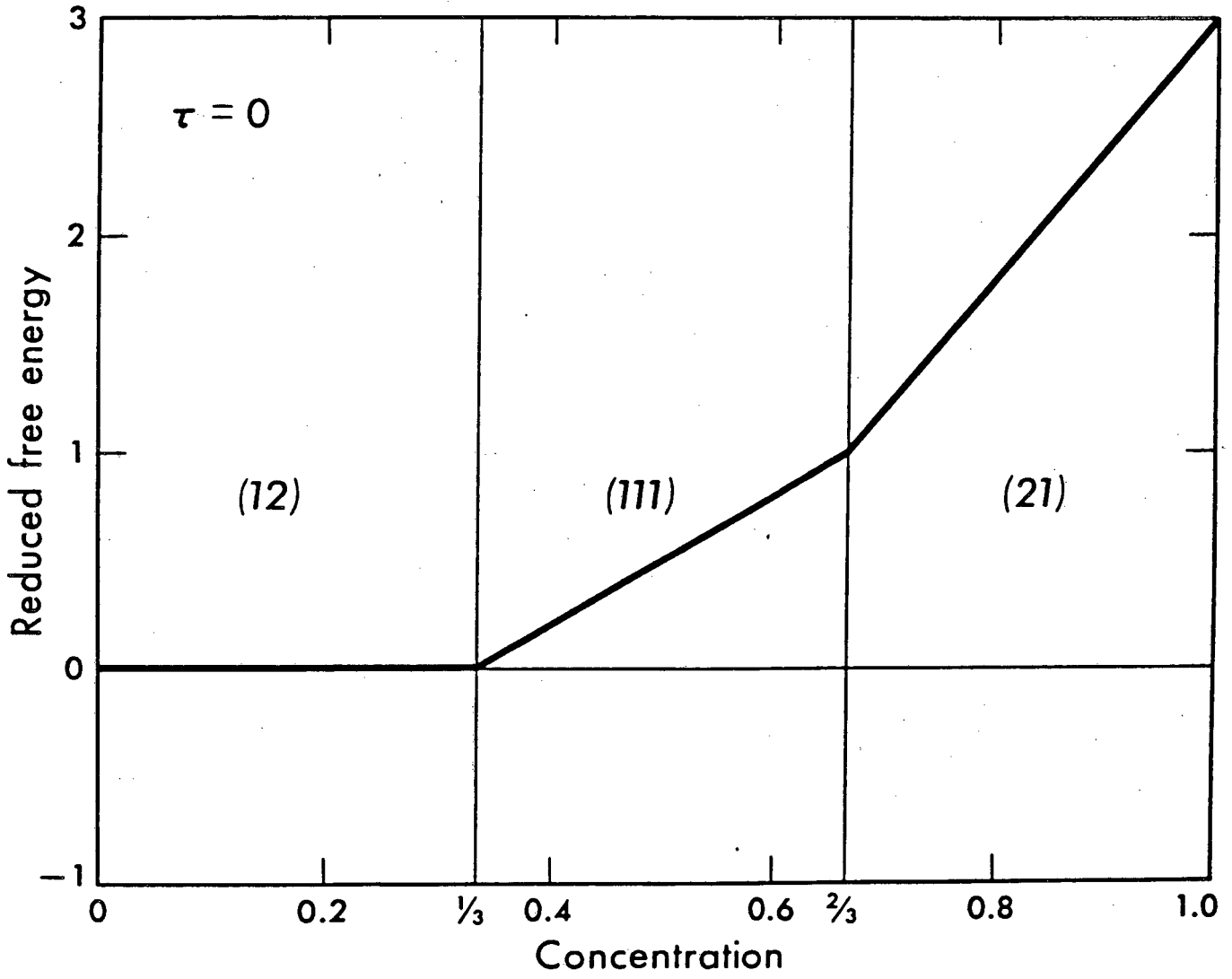
Figure 3.3

Generalized mean-field result for the reduced incremental
capacity multiplied by reduced temperature $(\tau \cdot \partial x/\partial \mu)$ as
a function of concentration $\underline{x}$ for (a) $\tau \to 0$, (b) $\tau=0.25$,
(c) $\tau=0.5$, (d) $\tau=0.7$. The dashed lines represent the
regular mean-field result of Eq. (3.14). In (a) this coin-
cides with the horizontal axis.
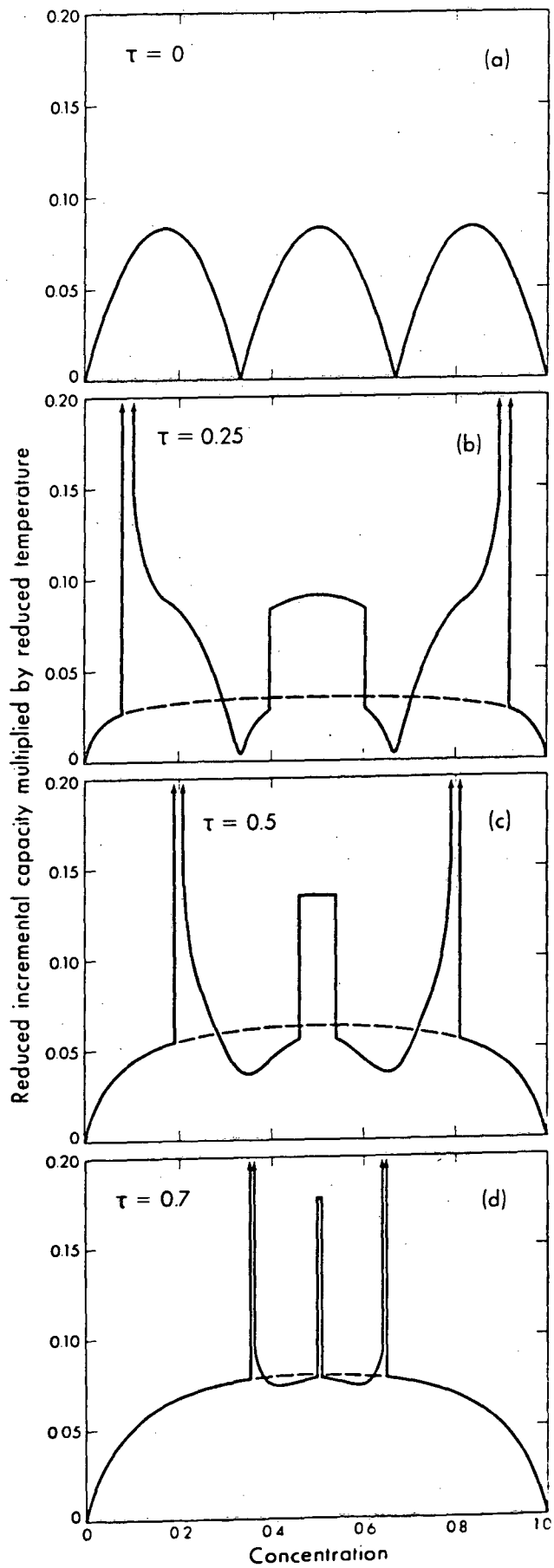
IV. <u>TRIANGLE-CLUSTER APPROXIMATION FOR Li$_x$TiS$_2$</u>

A. CALCULATION

In this chapter we develop the cluster-variation model for the triangular lattice gas introduced in sub-section II-B-3. The basic cluster is a nearest-neighbor three-sublattice triangle. The approximation was first used by Burley[1] to study antiferromagnetic behavior in an Ising model. While Burley assumed the distribution of spins on two of the sublattices to be equal, we give a more general solution,[2] including the possibility of three different site occupancies. Furthermore, we incorporate interactions between three particles in the model. This removes the artificial symmetry about $\underline{x}$ = 0.5 found in the phase diagram of the preceding chapter. We thus have here two adjustable parameters, namely the temperature and the three-body potential.

The expression for the interaction energy in Eq. (2.33) contains the nearest-neighbor repulsion $\underline{U}$ and the additional energy $U\phi$ for each closed nearest-neighbor triangle of atoms. We take ϕ to be negative in order to simulate the decreasing degree of ionization of the Li atoms in Li$_x$TiS$_2$ as $\underline{x}$ increases from 0 to 1. Nuclear-magnetic-resonance data[3] suggest that, while the ionization is essentially complete at small $\underline{x}$, 10 to 20% of an electron remains in the neighborhood of a Li atom at $\underline{x}$ = 1. Simple electrostatic arguments then suggest that ϕ takes values between (-0.3) and (-0.55).

Ground-state structures are found by minimizing the energy of Eq. (2.33) with respect to the triangle variables $\{z_{ijk}\}$, subject to the constraint of Eq. (2.18a) and an additional relation obtained from a well defined concentration:

$$x = \frac{1}{3}\left(x_1^\alpha + x_1^\beta + x_1^\gamma\right) \quad . \tag{4.1}$$

This is a typical problem of linear programming.[4] Ordered structures, corresponding to discontinuities in $(\partial\varepsilon/\partial x)$, result at $\underline{x} = 1/3$ and $2/3$, as in the generalized mean-field approximation, for $\phi > -1/2$. The structure at $\underline{x} = 2/3$ disappears for $\phi < -1/2$; the one at $\underline{x} = 1/3$ for $\phi < -3/2$: then the separation of all available particles into a phase of completely filled sites coexisting with a phase of empty sites becomes energetically favorable.

For finite temperatures we use Kikuchi's[5] "natural iteration" method to minimize the grand potential of Eq. (2.34), given μ, τ and ϕ. We define

$$\omega_O = \omega + \lambda\,(1 - \sum_{ijk} z_{ijk}) \quad , \tag{4.2}$$

where the Lagrange multiplier λ is used to introduce the constraint of Eq. (2.18a). The equations

$$\frac{\partial\omega_O}{\partial z_{ijk}} = 0 \tag{4.3}$$

lead to the superposition expression

$$z_{ijk} = \exp\left[\left(\lambda + \mu \, n_{ijk} - \varepsilon_{ijk}\right)/2\tau\right] Y_{ijk}^{1/2} X_{ijk}^{-1/6} \quad , \quad (4.4)$$

where for the <u>i</u>-<u>j</u>-<u>k</u> triangle configuration we define the number of particles per lattice site,

$$n_{ijk} = \frac{1}{3}\left(\delta_{i1} + \delta_{j1} + \delta_{k1}\right) \quad , \qquad (4.5)$$

the energy in units of <u>U</u> per lattice site,

$$\varepsilon_{ijk} = \delta_{i1}\,\delta_{j1} + \delta_{j1}\,\delta_{k1} + \delta_{k1}\,\delta_{i1}$$

$$(4.6)$$

$$+\, 2\phi\,\delta_{i1}\,\delta_{j1}\,\delta_{k1} \quad ,$$

(where δ_{mn} is Kronecker's delta) and the quantities

$$Y_{ijk} = y_{ij}^{\alpha\beta}\, y_{jk}^{\beta\gamma}\, y_{ki}^{\gamma\alpha} \qquad (4.7)$$

and

$$X_{ijk} = x_i^{\alpha}\, x_j^{\beta}\, x_k^{\gamma} \quad . \qquad (4.8)$$

In Eq. (4.4) the triangle probabilities are expressed as products of (a) the probabilities for the smaller clusters, (b) a Gibbs factor and (c) a normalization factor $\exp(\lambda/2\tau)$. The Lagrange multiplier λ can be identified with the minimized

grand potential, through the relation

$$\omega_O \equiv \omega_O - \sum_{ijk} z_{ijk} \frac{\partial \omega_O}{\partial z_{ijk}} = \lambda \quad . \tag{4.9}$$

The normalization relation of Eq. (2.18a) gives a cluster-variation approximation for the grand partition function Z as a sum over the triangle cluster, the Gibbs factor being weighted by the configuration probabilities of pairs and sites, in the form

$$Z^{1/2N} = \exp(-\lambda/2\tau) = \sum_{ijk} \exp\left[\left(\mu n_{ijk} - \varepsilon_{ijk}\right)/2\tau\right]$$

$$\times Y_{ijk}^{1/2} X_{ijk}^{-1/6} \quad . \tag{4.10}$$

The natural iteration calculation proceeds in the following steps: (a) initial values are chosen for the site and the pair variables (e.g., $x_1^\alpha = 0.8$, $x_1^\beta = 0.5$, $x_1^\gamma = 0.2$ for the ordered phases, and $x_1^\alpha = x_1^\beta = x_1^\gamma = 0.5$ for the disordered phase; $y_{ij}^{\alpha\beta} = x_i^\alpha x_j^\beta$ etc.); (b) a value of λ results from Eq. (4.10); (c) corresponding values for the set of triangle clusters $\{z_{ijk}\}$ are obtained from Eq. (4.4); (d) new values for $\{x_i^\nu\}$ and $\{y_{ij}^{\nu\nu'}\}$ are derived through the summation rules of Eqs. (2.18b) and (2.18c); (e) steps (b)-(d) are repeated until a convergence criterion is satisfied.

B. PHASE DIAGRAMS

We define the regions (3), (12), (21) and (111) in the

(x, τ) phase diagram as in Chapter III. For $\phi = 0$, the particle-hole symmetry discussed there holds and the (21) phase is the mirror image of the (12) phase about $x = 1/2$. This phase diagram is shown in Fig. 4.1. Comparing it with the Bragg-Williams phase diagram of the preceding chapter we notice two qualitative differences: (a) the triangle cluster-variation phase diagram shows a valley at $x = 1/2$ and (b) the disordered phase (3) continues to exist at $\tau = 0$. This topological evolution of the phase diagram as the approximation is improved parallels that for the fcc binary alloy, discussed by de Fontaine.[6]

For the first effect, we should notice that Wannier[7] has solved exactly the zero-field Ising antiferromagnet, and obtained a disordered stable phase. Our order-disorder coexistence region, which extends near $x = 1/2$ down to $\tau = 0.25$, should, with better approximations, continue to lower temperatures and include the $x = 1/2$, $\tau = 0$ point. The triangle cluster approximation, though better than the single-site approximation, still seems to be unreliable around $x = 1/2$ at low temperatures. The difference between the free energies of the different phases is very small in this region and the (111) phase happens to have a higher entropy.

The zero-temperature limit is usually avoided in cluster-variation calculations. Van Baal[8] justifies this practice with the argument that the approximations used in the ⌐

description of the energy, which is the predominant part of the free energy at low temperatures, makes the model lose contact with reality in this limit. We find the zero-temperature behavior to be of theoretical interest, however, to confirm the existence of the ground-state structures that led to the division of the lattice into sublattices. Our results show that the concentrations $x = 1/3$ and $2/3$ at $\tau = 0$ are second-order transition points between the phase (111) and the phases (12) and (21), respectively. For $x < 1/3$, the phases (3) and (12) have the same energy. The short-range correlations included in the cluster description allow for the existence of a disordered phase with zero energy at low concentrations. The intervals where each phase predominates are determined by the zero-temperature-limit entropies. The phases (3) and (12) coexist between $x = 0.2280$ and $x = 0.2515$. This interval corresponds to the first-order phase transition occuring in the lattice gas with infinite nearest-neighbor repulsion, treated by Burley.[9]

It has been proved[10] that the exact solution of the (3)-(12) order-disorder transformation in the triangular lattice with nearest-neighbor repulsions yields a second-order transition. The validity of the cluster-variation method as a hierarchy of approximations for this same model has been confirmed by McCoy et al.[11] They have shown that in the zero-temperature limit the value of the critical concen-tration and the behavior of the chemical potential and grand

potential approach the exact result[10] as the size of the

basic cluster increases.

In Fig. 4.2, the phase diagram for $\phi = -0.3$ illustrates

the asymmetry introduced by interactions between more than

two particles. The region of existence of the (21) phase

is significantly reduced, although the zero-temperature

behavior remains the same as for $\phi = 0$. Below $\phi = -0.5$,

however, the (21) phase and the ordered structure at $x = 2/3$

disappear altogether as discussed in the preceding section.

Such a behavior is displayed in the phase diagram of Fig. 4.3,

for $\phi = -0.6$. As $\tau \to 0$, the interval of coexistence between

the phases (12) and (3) extends to the whole interval between

$x = 1/3$ and $x = 1$.

C. THERMODYNAMIC FUNCTIONS

We discuss the behavior of the reduced entropy and the

reduced incremental capacity, and compare the latter to

experimental results for systems like Li_xTiS_2.

The entropy at fixed temperature as a function of the

concentration shows minima at small τ where ordered structures

occur. The negative three-particle potential increases the

values of the entropy for $x > 1/2$. These two effects are

illustrated in Fig. 4.4, where results are presented for

several temperatures at $\phi = -0.3$, which corresponds to an

ionization of 90% at $x = 1$.

In regards to the incremental capacity, our results

also show minima at concentrations where ordered structures

are expected, as in the generalized mean-field approximation. We are able to account also for the peaks in the experimental data[12] for $Li_x TiS_2$ at $x = 1/9$ and $1/4$. For any ϕ and $\tau < 0.2$ a smooth maximum appears near $x = 1/9$. The point $x = 1/4$ is inside the small interval where a diverging incremental capacity indicates an order-disorder transition. A smooth maximum near $x = 6/7$ can be reproduced for $\phi = -0.3$, $\tau = 0.2$. The negative three-particle interaction produces high values for the incremental capacity in the disordered phase for $x > 1/2$. In Fig. 4.5, results are presented for $\phi = -0.3$ and several temperatures, together with Thompson's results[12] for $Li_x TiS_2$, where the mentioned peaks are observed, and for $Li_x Ta_{0.8} Ti_{0.2} S_2$, where minima at $x = 1/3$ and $2/3$ occur.[13]

A nearest-neighbor approximation in a triangular lattice gas can thus account semi-quantitatively for the experimental features in the incremental capacity for lithium intercalation in some transition-metal dichalcogenides. We should mention that a cluster-variation calculation cannot predict the correct analytical behavior of thermodynamic functions at critical points, although their location in the phase diagram can be predicted with satisfactory accuracy.

D. CONCLUSIONS

We have presented in the chapter order-disorder phase diagrams for the triangular lattice gas with nearest-neighbor pairwise repulsive and three-particle attractive interactions. The main effect of the three-particle parameter is to decrease

the temperature range of existence of the ordered phase corresponding to the structure at x = 2/3, thus removing the particle-hole symmetry found in the preceding chapter. This is reflected in the curves for the entropy and the incremental capacity as functions of the concentration. The qualitative picture given in the preceding chapter for the minima and maxima of the incremental capacity is confirmed. Furthermore, we are able to reproduce quantitatively the position of maxima and minima of the experimental data.

We thus confirm the validity of the lattice gas model as a first approximation for the problem of ordering of Li^+ ions in systems like $Li_x TiS_2$. Better results can almost certainly be achieved by introducing longer-range interactions. The improvements, however, are limited mainly by the inaccurate description of the guest-host interaction and the electronic contributions due to the filling of the TiS_2 conduction band.

REFERENCES: CHAPTER IV

1. D.M. Burley, Proc. Phys. Soc. (London) 85, 1163 (1965).

2. R. Osório and L.M. Falicov, J. Phys. Chem. Solids 43, 73 (1982).

3. Chapter I, ref. 20.

4. See, e.g. G.B. Dantzig, Linear Programming and Extensions (Princeton University, Princeton, 1965).

5. Chapter II, ref. 6.

6. Chapter II, ref. 2.

7. G.H. Wannier, Phys. Rev. 79, 357 (1950).

8. Chapter III, ref. 3.

9. D.M. Burley, Proc. Phys. Soc. (London) 85, 1173 (1965).

10. R.J. Baxter, J. Phys. A 13, L61 (1980).

11. Chapter II, ref. 4.

12. Chapter I, refs. 24, 25.

13. Chapter I, ref. 27.

Figure 4.1

Phase diagram in the (x, τ) plane for the triangular lattice gas in the triangle approximation with nearest-neighbor repulsions only.
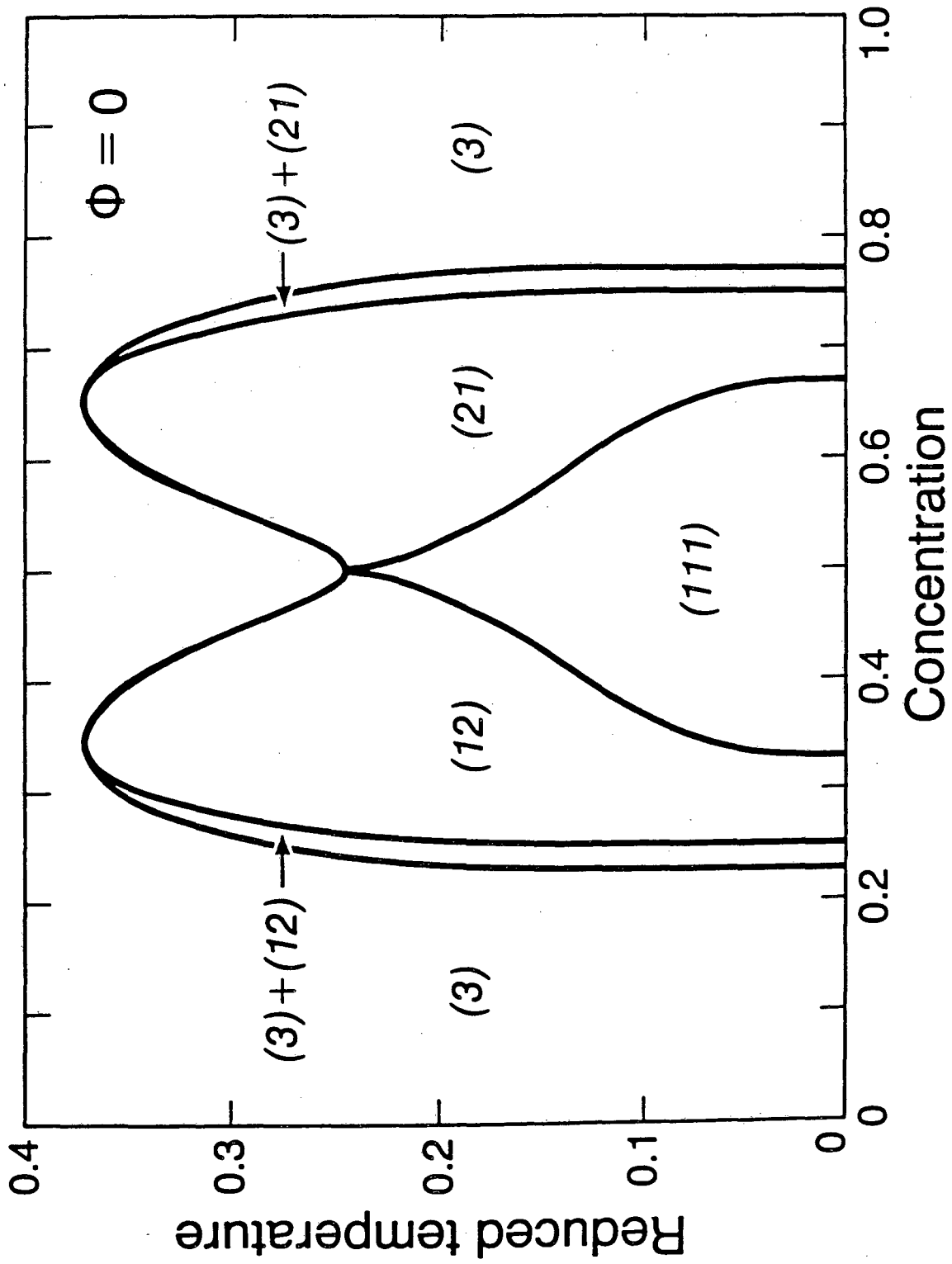
Figure 4.2

Phase diagram in the (x,τ) plane for the triangle lattice gas with a three-particle parameter $\phi = -0.3$. Horizontal lines are drawn for $\tau = 0.1$, 0.2 and 0.3 so that the behavior of the constant-temperature thermodynamic functions of Figs. 4.4 and 4.5 can be compared with the phase diagram.
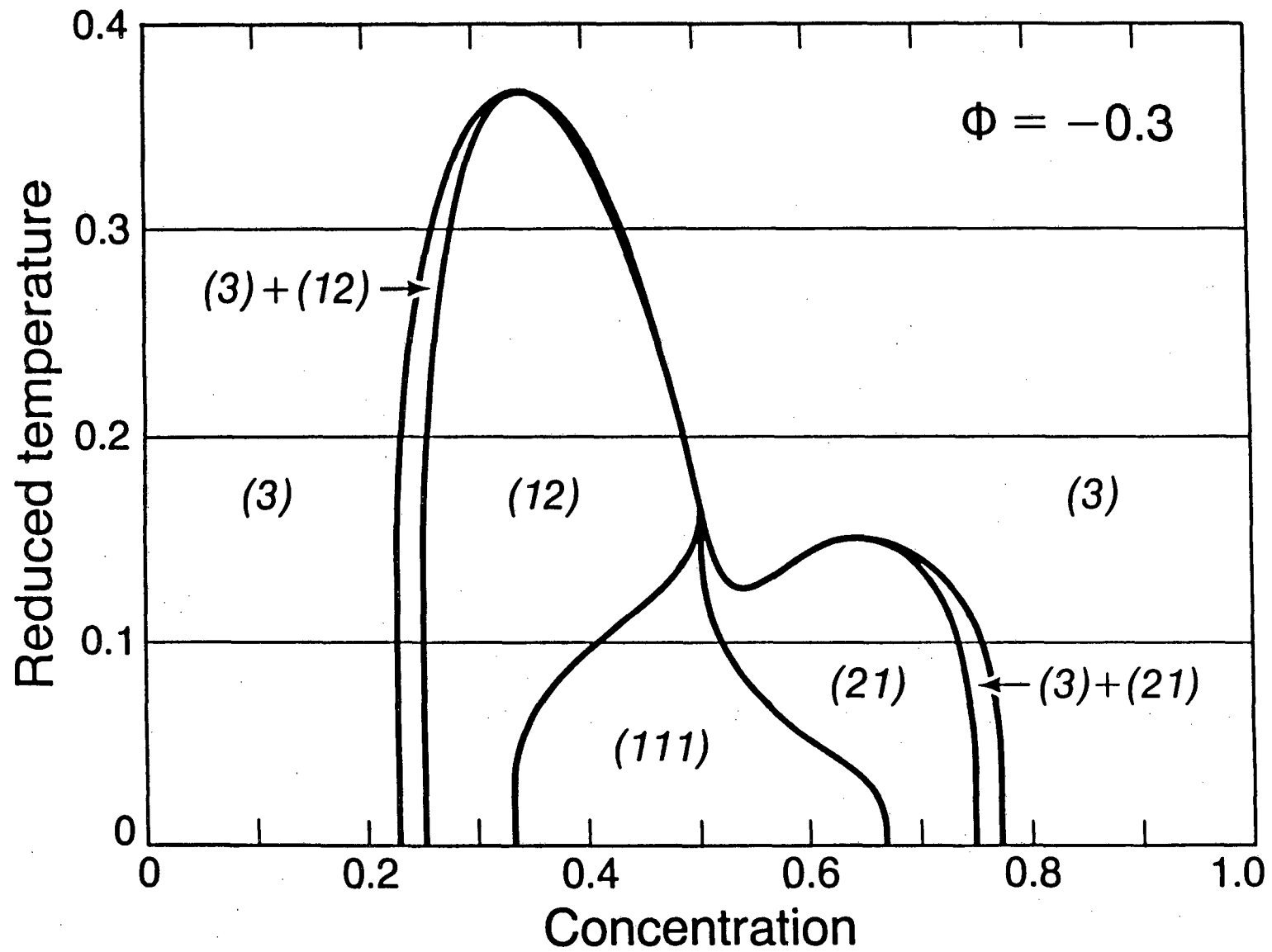
Figure 4.3

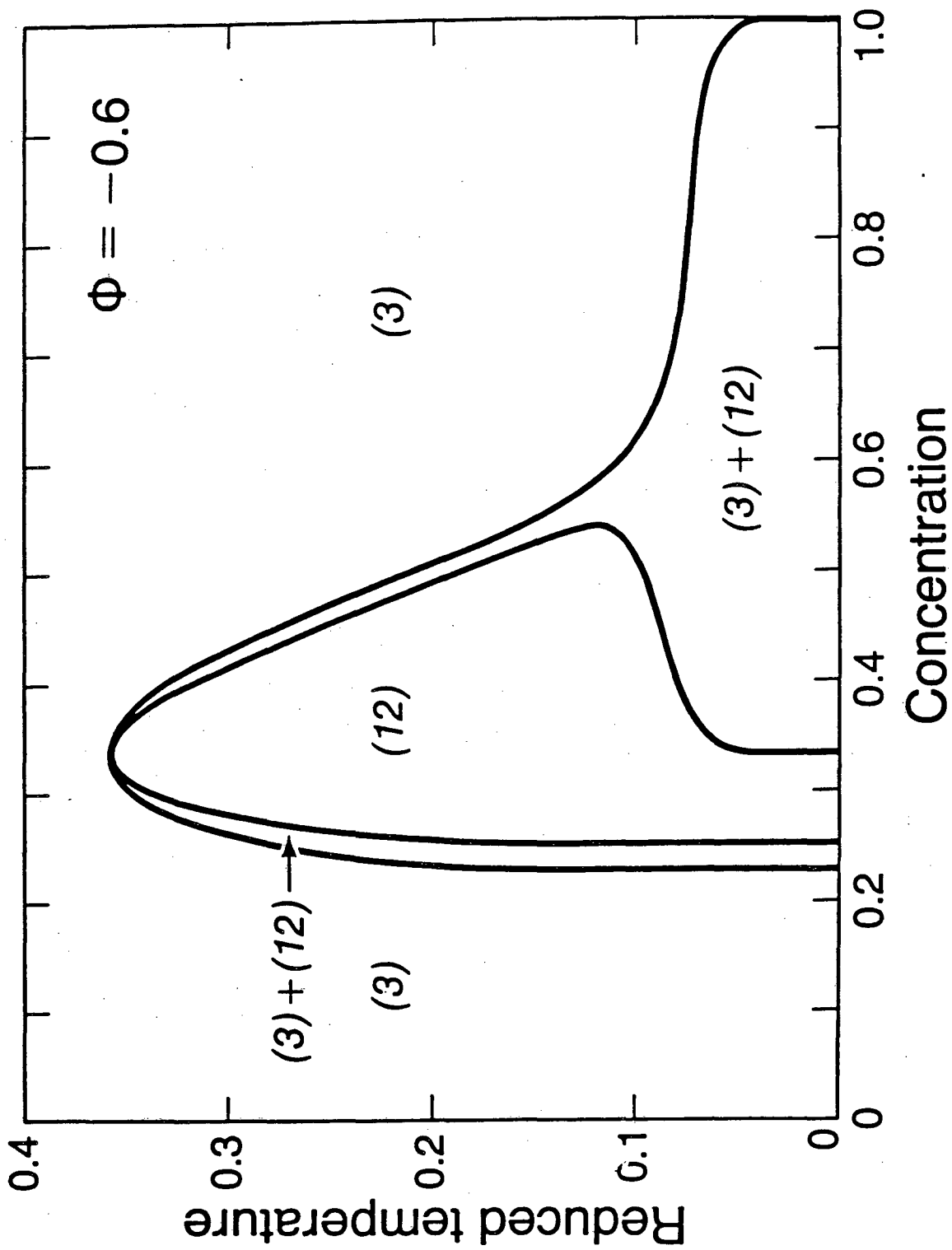Phase diagram in the (x, τ) plane for the triangular lattice gas with a three-particle parameter $\phi = -0.6$.

Figure 4.4

Reduced entropy and molar entropy (in J mol^{-1} K^{-1}) as functions of concentration for a three-particle parameter $\phi = -0.3$ and several values of the reduced temperature τ. Arrows indicate second-order transition points for $\tau = 0.1$. This Figure corresponds to the phase diagram of Figure 4.2.

Figure 4.5

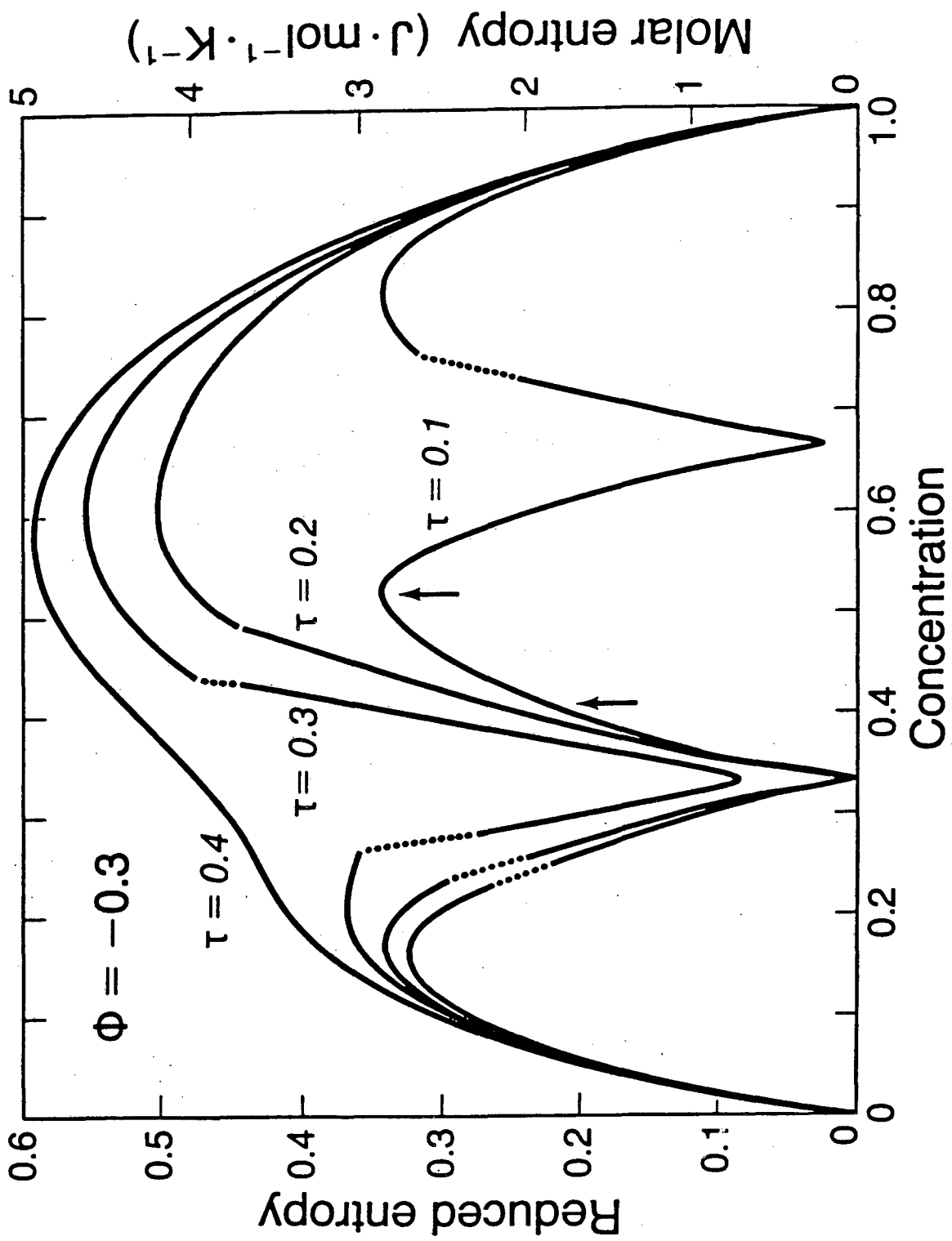Reduced incremental capacity multiplied by the reduced temperature $(\tau \cdot \partial x / \partial \mu)$ and incremental capacity (in volts $^{-1}$ assuming T = 300K) for ϕ = -0.3 and (a) τ = 0.1, (b) τ = 0.2, (c) τ = 0.3, (d) τ = 0.4 and the experimental results for (e) $Li_x TiS_2$ and (f) $Li_x Ta_{0.8} Ti_{0.2} S_2$ from Ref. 13. In (a) arrows indicate second-order transition points.

Reduced incremental capacity multiplied by reduced temperature

Incremental capacity at room temperature (volts^{-1})

Concentration

(a) $\Phi = -0.3$, $\tau = 0.1$ — 1/9, 1/4

(b) $\Phi = -0.3$, $\tau = 0.2$ — 1/9, 1/4, 6/7

(c) $\Phi = -0.3$, $\tau = 0.3$

(d) $\Phi = -0.3$, $\tau = 0.4$

(e) Li$_x$TiS$_2$ — 1/9, 1/4, 6/7

(f) Ta$_{0.8}$Ti$_{0.2}$S$_2$

-71-
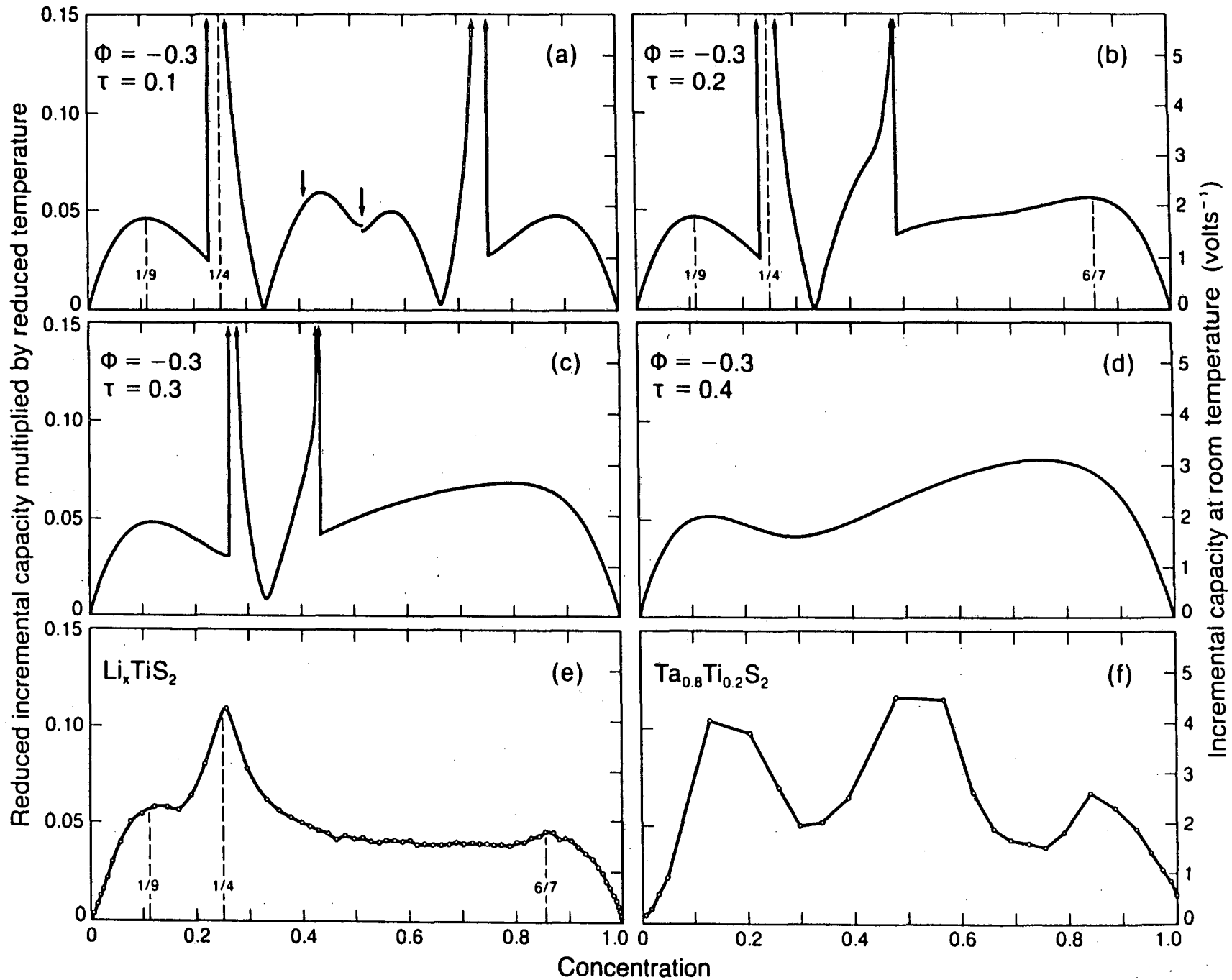
V. THE EFFECTS OF A RANDOM DISTRIBUTION OF DIFFERENT SPECIES OF HOST ATOMS

A. INTRODUCTION

As discussed in Chapter I, Thompson[1] has obtained voltage-composition relations for several values of y in $Li/Ta_yTi_{1-y}S_2$ batteries. Strikingly different results between the cases $y = 0$ and $y = 1$ indicate different types of interactions between Li ions when intercalated in TiS_2 and TaS_2 with a possible strong contribution of crystal distortions for TaS_2.[2,3] On the other hand, for $y \leq 0.5$ the main effects of the substitution of Ta for Ti atoms in the host are lower values for the voltage for all x and smoother incremental capacity curves. It is clear that different guest-host interactions play an important role in the evolution of such incremental capacity curves as y is increased.

In this chapter we study a general mean-field theory for the triangular lattice gas with different types of site energies randomly distributed along the lattice. As in the preceding chapters, the atoms interact through a nearest-neighbor repulsion, and a three-sublattice representation is used. The different site energies are intended to represent different guest-host interactions. The model is applied to $Li_xTa_yTi_{1-y}S_2$, although it can be generalized in a straightforward way to other intercalation materials where different species of host atoms are randomly distributed.

B. GENERALIZED MEAN-FIELD THEORY FOR RANDOMLY DISTRIBUTED SITE ENERGIES

In the case of $Li_xTa_yTi_{1-y}S_2$, we consider only the effect of the transition-metal atoms directly above and below each site available for Li occupation. We divide the lattice into three "chemical types" with energy E_σ and number of sites (Np_σ). Here $\sigma = 0,1,2$ denotes the sites that lie between two Ti atoms $\left[p_0=(1-y)^2\right]$, between one Ta and one Ti $\left[p_1=2y(1-y)\right]$, and between two Ta $\left[p_2=y^2\right]$. We also assume that the replacement of a Ta for a Ti contributes a term E_1 to E_σ, so that

$$E_\sigma = E_0 + \sigma E_1 \quad . \tag{5.1}$$

The value of E_0 contributes a constant voltage to the voltage-composition relations and does not affect the form of the incremental capacity curves. Therefore we take $E_0 = 0$ for simplicity.

Since the voltage drops in general when y increases, we can conclude that Li is less easily intercalated when Ta atoms replace Ti atoms. This indicates a positive value for E_1 in Eq. (5.1). We estimate $E_1 \sim 10^{-1}$ eV from the difference between the free energies of formation[1] (i.e. the integrals of the voltage-composition relations) of Li_1TiS_2 and Li_1TaS_2. This is of the same order of magnitude of the nearest-neighbor repulsion U between the Li ions

required for a reasonable fitting of the incremental capac-
ity of $Li_x TiS_2$ by the cluster-variation calculation of the
preceding chapter. We must keep in mind that $\underline{U}$ can depend
on $\underline{y}$, since different host lattices contribute differently
to the screening of the Li-Li repulsion. The dependency
of $\underline{U}$ on $\underline{x}$, simulated in the preceding chapter by the three-
atom interaction, is neglected in the present discussion.

In the three-sublattice representation of Chapter II,
each of the sublattices ν has a number $(Np_\sigma/3)$ of sites of
chemical type σ and, by definition, $(Nd_{\nu\sigma}/3)$ such sites
that are occupied. We also define (Nc_σ) as the total number
of sites of chemical type σ that are occupied. As in
Chapter III, n_ν is the total fractional occupation of sub-
lattice ν. Table 5.1 summarizes this notation. The follow-
ing constraints hold for the occupation variables $d_{\nu\sigma}$:

$$0 \leq d_{\nu\sigma} \leq p_\sigma \; ; \tag{5.2a}$$

$$\sum_\nu d_{\nu\sigma} = 3c_\sigma \; ; \tag{5.2b}$$

$$\sum_\sigma d_{\nu\sigma} = n_\nu \; ; \tag{5.2c}$$

$$\sum_{\nu\sigma} d_{\nu\sigma} = 3x \; . \tag{5.2d}$$

The statistical weight for the entropy, in the mean-
field approximation, is

$$g = \prod_{\nu\sigma} \frac{(Np_\sigma/3)!}{(Nd_{\nu\sigma}/3)![N(p_\sigma-d_{\nu\sigma})/3]!} \quad , \tag{5.3}$$

while the reduced energy (in the notation of Chapter II) is approximated by

$$\epsilon = n_\alpha n_\beta + n_\beta n_\gamma + n_\gamma n_\alpha + \sum_\sigma \psi_\sigma c_\sigma \quad , \tag{5.4}$$

where we define

$$\psi_\sigma \equiv \frac{E_\sigma}{U} = \frac{\sigma E_1}{U} \quad . \tag{5.5}$$

Given $\underline{y}$, μ, τ and ψ_1, the nine occupation probabilities $\{d_{\nu\sigma}\}$ are independent variables for the minimization of the reduced grand potential

$$\omega = \frac{9}{2} x^2 - \mu x - \frac{1}{2} \sum_\nu n_\nu^2 + \sum_\sigma \psi_\sigma c_\sigma$$
$$+ \frac{\tau}{3} \sum_{\nu\sigma} \left[L(d_{\nu\sigma}) + L(p_\sigma - d_{\nu\sigma}) - L(p_\sigma) \right] \quad , \tag{5.6}$$

where the operator L was defined in Eq. (2.35).

A finite-temperature minimization method for ω is discussed in Section D. In the following section we examine the zero-temperature case.

C.   GROUND-STATE DIAGRAMS

At zero temperature the present model can be solved by

minimizing the quadratic form (5.4) for the energy with the restrictions of Eq. (5.2), at given $\underline{y}$, $\underline{x}$ and ψ_1. This problem can in principle be solved by the methods of "quadratic programming".[4]

A simpler scheme can be devised by noticing that, in general, the solution defines a point in the $d_{\nu\sigma}$-space where all but one of the $\{d_{\nu\sigma}\}$ either are zero or assume their maximum possible value p_σ. Given $\underline{y}$ and ψ_1, the concentration ($\underline{x}$) axis is then divided into several intervals, each of them having only one $d_{\nu\sigma}$ varying (linearly) with $\underline{x}$. This picture is always valid for small or large ψ_1, compared to unity. For $\psi_1 \sim 1$, however, the curve (i.e., the broken line) ε vs. $\underline{x}$ is not always concave. Lines of lower energy can then be drawn which are tangents to the original curve. This procedure defines intervals of coexistence of phases. Once this method is applied to many values of ψ_1, at given $\underline{y}$, a phase diagram can be obtained in the (x, ψ_1) plane.

In practice such calculations can be simplified by the observation that there are only three independent sequences for filling the $\{d_{\nu\sigma}\}$ (in the case where $\sigma = 0,1,2$) as one fills the lattice from $x = 0$ to 1. These sequences are (we only keep the indices $\nu\sigma$ of $d_{\nu\sigma}$ in the following discussion)

$$\alpha 0 - \alpha 1 - \alpha 2 - \beta 0 - \beta 1 - \beta 2 - \gamma 0 - \gamma 1 - \gamma 2 \, , \qquad \text{(a)}$$

$$\alpha 0 - \alpha 1 - \beta 0 - \beta 1 - \gamma 0 - \gamma 1 - \alpha 2 - \beta 2 - \gamma 2 \, , \qquad \text{(b)}$$

$$\alpha 0 - \beta 0 - \gamma 0 - \alpha 1 - \alpha 2 - \beta 1 - \beta 2 - \gamma 1 - \gamma 2 \, . \qquad \text{(c)}$$

Other sequences can be derived from these three basic ones.
For instance, the sequence

$$\alpha 0 - \beta 0 - \gamma 0 - \alpha 1 - \beta 1 - \gamma 1 - \alpha 2 - \beta 2 - \gamma 2 \qquad (d)$$

is indentical to sequence (c) until $\alpha 1$ is filled and to
sequence (b) once $\gamma 1$ starts to be filled. Between the two
cases, filling $\beta 1$ is equivalent to taking a two-phase mixture,
with one phase following sequence (c) with $\alpha 0 - \beta 0 - \gamma 0 - \alpha 1$
filled (the rest empty) and the other phase following sequence
(b) with $\alpha 0 - \alpha 1 - \beta 0 - \beta 1 - \gamma 0$ filled (the rest empty).
Equations for ε as a function of $\underline{x}$ for the three basic
sequences can be obtained in a straightforward way from
Eq. (5.4). At given $\underline{y}$ and ψ_1, the three curves are then
compared and the tangent method is used when necessary.

This procedure leads to ground-state diagrams in the
(x, ψ_1) plane like those shown in Fig. 5.1 for several values
of $\underline{y}$. Shaded regions represent two-phase mixtures. For
each single-phase region the indices $\nu\sigma$ give the only occupa-
tion variable $(d_{\nu\sigma})$ that varies with $\underline{x}$, while all others
equal either 0 or p_σ. While the diagrams are relatively
simple for certain values of $\underline{y}$ like 1/2 and 1/3, they become
quite elaborate for general values of $\underline{y}$. The symmetry of
the equation for the energy allows us to obtain diagrams
for $y > 1/2$ from the ones for $y < 1/2$. The diagram for
$(1-y)$ results from reversing the diagram for $\underline{y}$ about

$x = 1/2$; in the notation for the single-phase regions we must also change $\alpha \leftrightarrow \gamma$ and $0 \leftrightarrow 2$.

The fundamental feature of the phase diagrams of Fig. 5.1 is the stability of sequence (a) for $\psi_1 \ll 1$ and of sequence (d) for $\psi_1 \gg 1$. In the first case the sublattices are completely filled in succession. In the second case the division into chemical types predominates over the sublattice representation, and there are spatially disordered ground-state structures at $x = p_0, p_0 + p_1$.

In the single-phase intervals (at given $\underline{y}$ and ψ_1), the free energy becomes a smooth function of $\underline{x}$ at finite τ. The zero-temperature incremental capacity is determined by the limiting behavior of the entropy. Between two critical points, x_n and x_{n+1}, that determine a ground-state single-phase interval, we have

$$\lim_{\tau \to 0} \tau \frac{\partial x}{\partial \mu} = \frac{(x - x_n)(x_{n+1} - x)}{x_{n+1} - x_n} \quad , \tag{5.7}$$

i.e., a simple parabola with roots at $x = x_n, x_{n+1}$ and slope ± 1 at these points. On the other hand, the two-phase regions are expected to survive for small non-zero values of τ; the free energy for those regions remains a linear function of τ and $(\tau \cdot \partial x / \partial \mu)$ diverges. A typical zero-temperature form of the incremental capacity, with one- and two-phase intervals, is shown in Fig. 5.2 for $y = 1/3$, $1/3 < \psi_1 < 1/2$.

D. FINITE-TEMPERATURE CALCULATION

The minimization of ω in Eq. (5.6) with respect to the $\{d_{\nu\sigma}\}$ yields the following expression after some simple algebraic manipulation:

$$d_{\nu\sigma} = \frac{P_\sigma}{\exp\{[\psi_\sigma + 3(3x - n_\nu) - \mu]/\tau\} + 1} \qquad (5.7)$$

Thus, the occupation variables $d_{\nu\sigma}$ obey a Fermi-Dirac distribution, with the appropriate mean-field approximation $U[\psi_\sigma + 3(3x - n_\nu)]$ for the energy of an occupied site designated by the indices $\nu\sigma$. This type of Fermi-Dirac distribution can be easily understood, since each site of the lattice can be either empty or occupied by at most one particle.

The set of equations given by (5.7) is reducible to a set of equations of only one variable through a summation over the chemical types σ. The result is

$$h(n_\nu) \equiv n_\nu - \sum_\sigma \frac{P_\sigma}{\exp\{[\psi_\sigma - 3(n_\nu + \lambda)]/\tau\} + 1} = 0 \quad , \qquad (5.8)$$

where we define

$$\lambda = -3x + \frac{\mu}{3} \quad . \qquad (5.9)$$

Eq. (5.8) is similar to Eq. (3.6); both have three roots in general. Phase diagrams in the (x, τ) plane can be obtained in the present case, at given y and ψ_1, by the method of Chapter III.

E. PHASE DIAGRAMS AND INCREMENTAL CAPACITY

For $y = 1/2$, the phase diagram in the (x, τ) plane is symmetric about $x = 1/2$, for any value of the site energy parameter ψ_1. In Fig. 5.3, the order-disorder curves for the $\psi_1 = 1/4$ and 4 illustrate the additional disorder introduced into the system by the quenched disorder in the distribution of different species of host atoms. The main effect of a small finite ψ_1 is a quadratic decrease of the critical temperature for the order-disorder transition at $x = 1/2$, from the value $\tau_c = 0.75$ at $\psi_1 = 0$. This last case is shown in Fig. 2.1. On the other hand, large values of ψ_1 lead to topologically different phase diagrams; depending on the value of τ, we can have alternate intervals of order and disorder as x increases from 0 to 1. The critical temperature τ_c at $x = 1/2$ for $y = 1/2$ is plotted in Fig. 5.4 as a function of ψ_1; τ_c drops from 3/4 at $\psi_1 = 0$ to 3/8 as $\psi_1 \to \infty$.

Simple physical interpretations can be given to the features of incremental capacity curves obtained from the present model. We show in Fig. 5.5(a) the results for $y = 0.8$, $\psi_1 = 2$, $\tau = 0.4$. In this case, there is only one interval where spatically ordered phases are stable, between $x \approx 0.52$ and $x \approx 0.82$. The divergences at these points are due to order-disorder transitions. The two minima within the order interval are caused by the appearance of long-range ordered structures when sites of the highest-energy chemical type $(\sigma = 2)$ are being filled. The other two

minima or dimples, at values of x close to $(1-y)^2 = 0.04$ and $(1-y^2) = 0.36$ are caused by another type of ordering, associated with the nearly complete filling of the chemical types $\sigma = 0$ and 1.

Because it is a mean-field theory, the present model is expected to be more accurate when the correlations between sites are not important, i.e., in the spatially disordered phase. In fact we get better agreement with the experimental data for $Li_xTa_yTi_{1-y}S_2$ for $0.1 < y < 0.5$, where smooth incremental capacity curves obtained by Thompson[1] suggest a disordered distribution of Li ions. We show the results for $y = 0.3$ in Fig. 5.5(b), with our input parameters $\psi_1 = 3$, $\tau = 0.75$, together with Thompson's experimental data.

F. CONCLUSIONS

In this chapter we have studied the influence of a quenched random distribution of different species of host atoms on the order-disorder phase diagram of the intercalate ions. The mean-field model for the spatially disordered phase gives a reasonable approximation for the incremental capacity curves of the Ti-rich end of the $Li_xTa_yTi_{1-y}S_2$ series. It is doubtful whether any rigid-lattice model can accurately describe the behavior on the Ta-rich end, where crystal distortions in the host may play an important role.

Although the order-disorder phase diagrams are not expected to be accurate in the mean-field approximation,

the present model results in interesting physical features,
like the existence of minima in the incremental capacity
due to two different kinds of ordering of the particles.
There is a spatial ordering that results from filling the
sublattices one by one, and a "chemical type" ordering
that results from filling the sites with different chemical
environment in the sequence of the values of their site
energies. In addition, divergences of the incremental
capacity can also be due to two distinct kinds of coexis-
tence of phases: one occurring about an order-disorder
transition, like in Fig. 5.5(a), and the other resulting
from the coexistence of two ordered phases, like in Fig. 5.2.

REFERENCES: CHAPTER V

1. Chapter I, ref. 27.

2. Chapter I, ref. 14.

3. A.H. Thompson, Phys. Rev. Lett. $\underline{34}$, 520 (1975).

4. See, e.g., L.C.W. Dixon, Nonlinear Optimization (English Universities, London 1972).

Table 5.1
Notation for the variables in Eq. (5.2).

	On sublattice ν	On chemical site of type σ	On chemical site of type σ, sublattice ν
Total number of sites	$\dfrac{N}{3}$	Np_σ	$\dfrac{N}{3} p_\sigma$
Number of occupied sites	$\dfrac{N}{3} n_\nu$	Nc_σ	$\dfrac{N}{3} d_{\nu\sigma}$

Figure 5.1

Ground-state mean-field phase diagrams in the (x, ψ_1) plane for the triangular lattice gas with three sublattices and three chemical types, for (a) y = 0.2, (b) 1/3 and (c) 0.5.

(a) y = 0.2

(b) y = ⅓

(c) y = 0.5
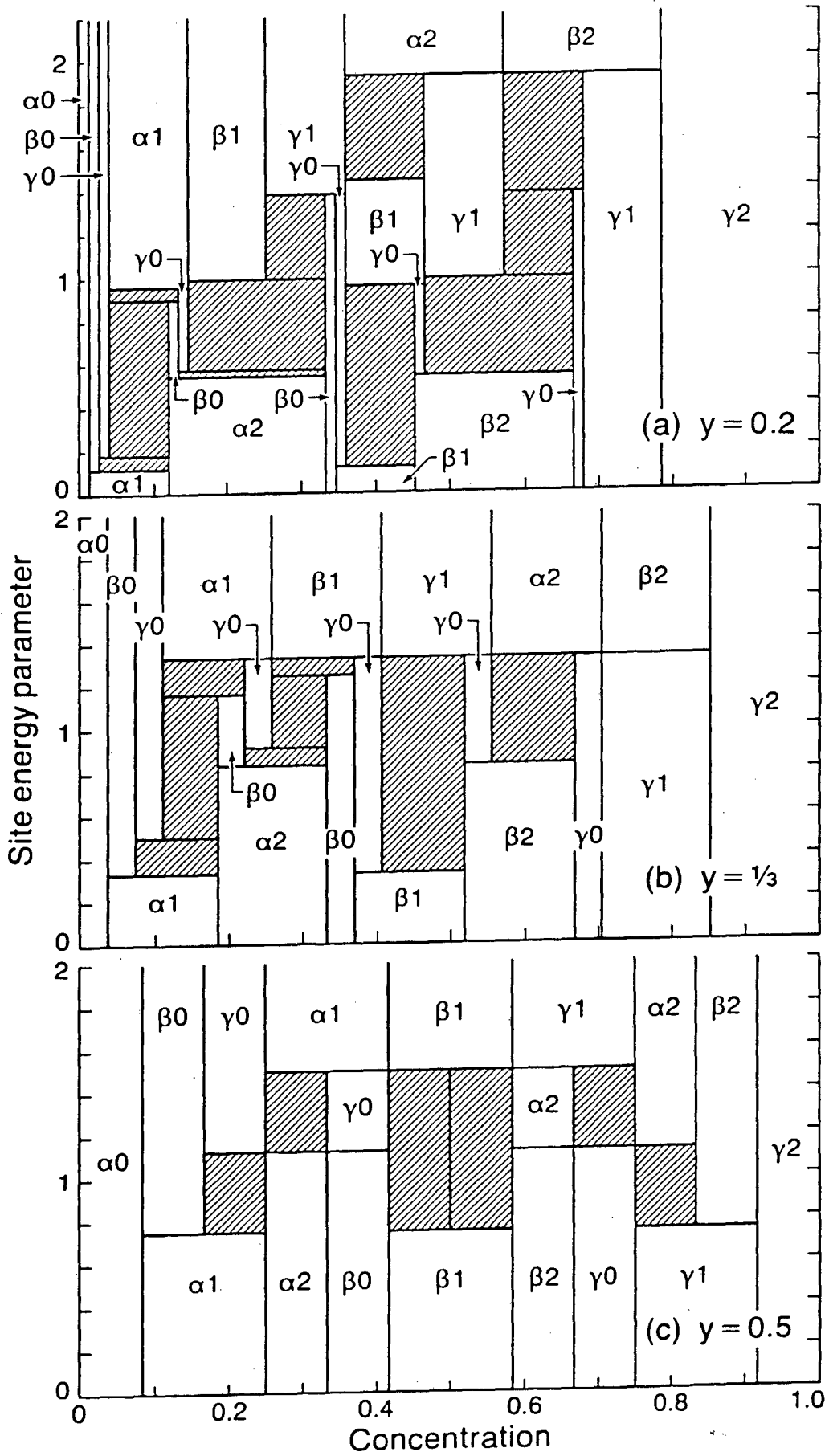
Figure 5.2

Zero-temperature limit of the reduced incremental capacity
multiplied by reduced temperature $(\tau \cdot \partial x / \partial \mu)$ for $y = 1/3$,
$1/3 < \psi_1 < 1/2$.
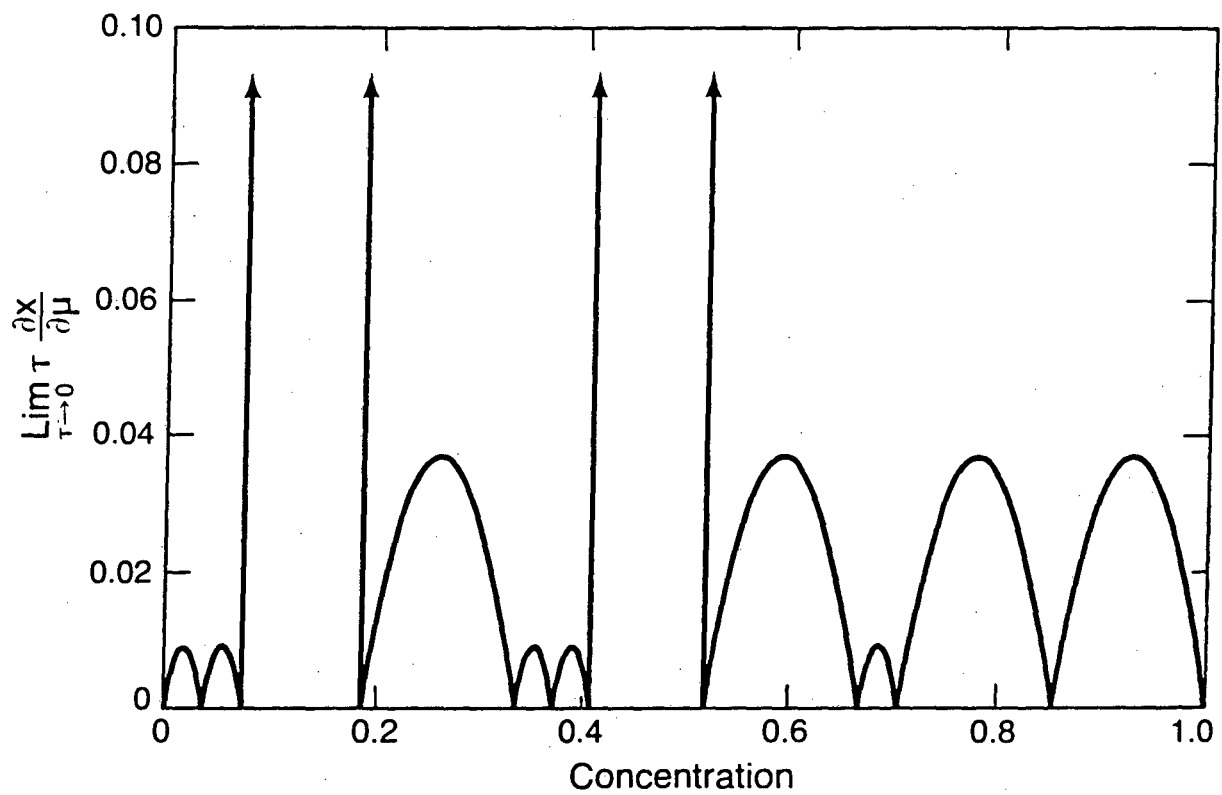
Figure 5.3

Phase diagrams in the (x, τ) plane with a site energy

parameter ψ_1 = 1/4 and 4, for y = 1/2. For each ψ_1,

the disordered phase is stable above the upper curve

and ordered phases occur below the lower curve; the

narrow bands between the two curves are regions of order-

disorder phase coexistence. An arrow indicates the

critical temperature τ_c = 3/4, the maximum τ (at x = 1/2)

for similar curves with ψ_1 = 0.

(a) $\psi_1 = \frac{1}{4}$

(b) $\psi_1 = 4$

$y = 0.5 \longrightarrow$

Reduced temperature

Concentration
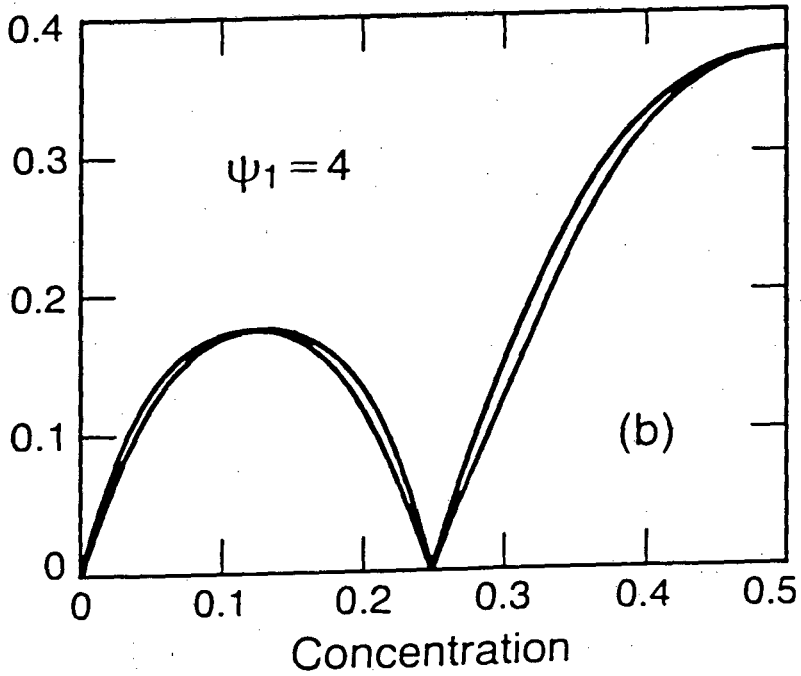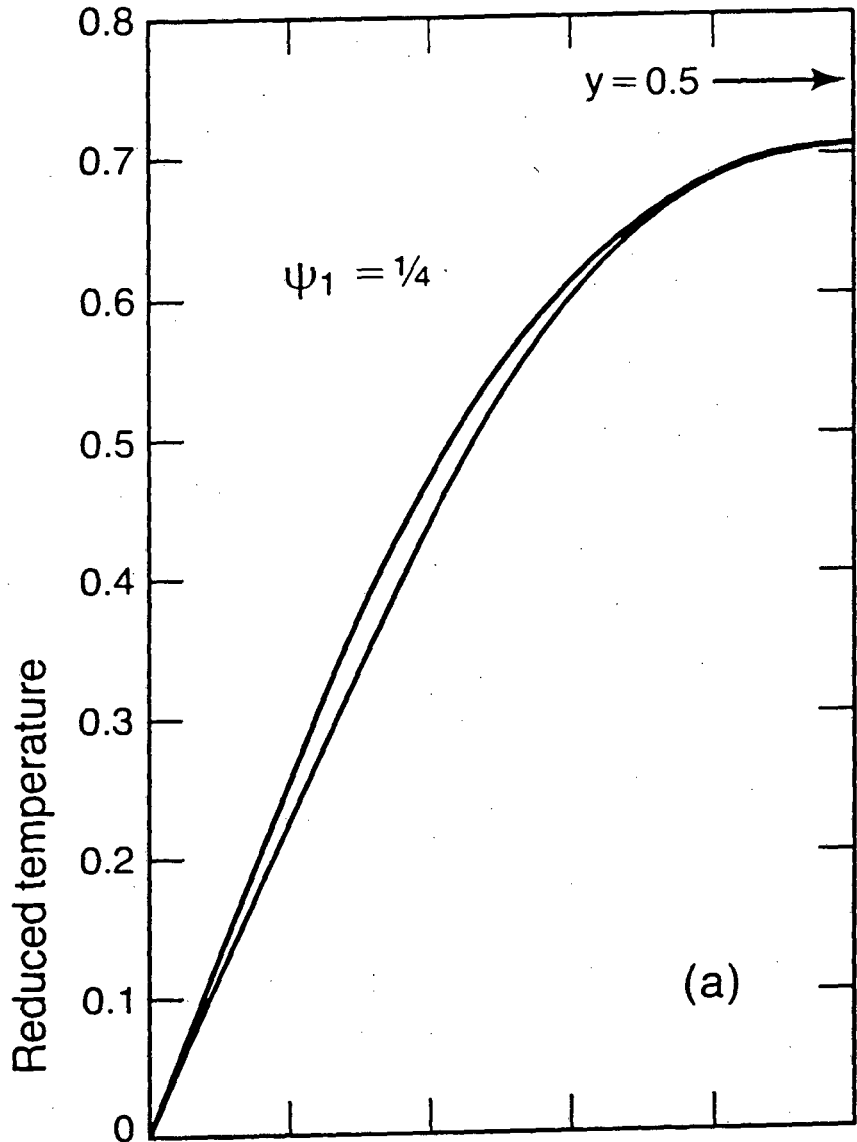
Figure 5.4

Reduced critical temperature for the order-disorder transition at x = 1/2 for y = 1/2 as function of the site energy parameter ψ_1.
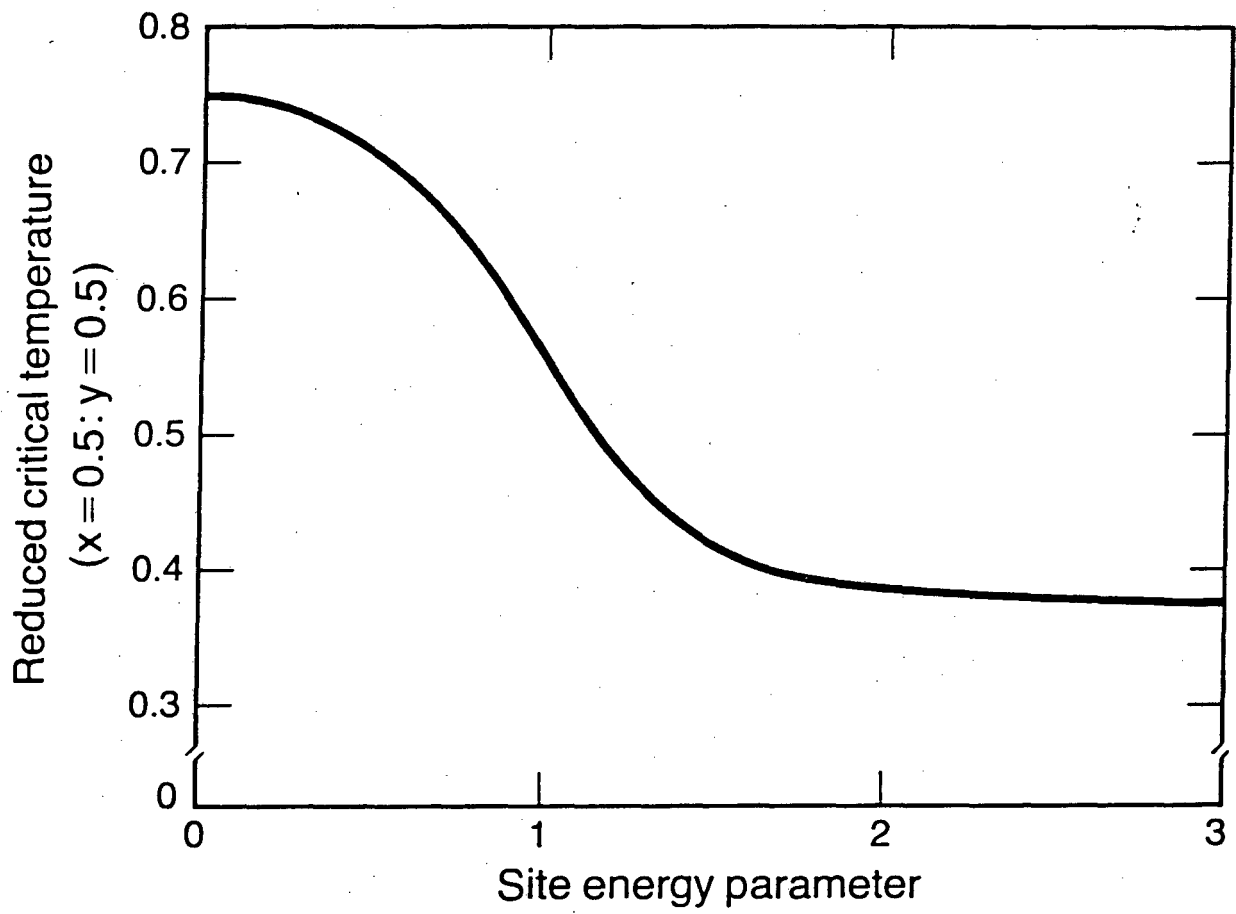
Figure 5.4

Figure 5.5

Reduced incremental capacity multiplied by reduced temperature for (a) $y = 0.8$, $\psi_1 = 2$, $\tau = 0.4$; (b) $y = 0.3$, $\psi_1 = 3$, $\tau = 0.75$. In (b) the circles are the experimental data of Thompson (ref. 1) for $Li_x Ta_{0.3} Ti_{0.7} S_2$.